1 **Structure and mechanism of mitochondrial proton-translocating**

2 **transhydrogenase**

3 Domen Kampjut and Leonid Sazanov*

4

5     Proton-translocating transhydrogenase (NNT), found in the plasma membranes of

6 bacteria and in the inner mitochondrial membranes, catalyses the proton translocation-

7 coupled transhydrogenation $NADH + NADP^+ + H^+_{out} <-> NAD^+ + NADPH + H^+_{in}$.

8 Its physiological function is the generation of NADPH for anabolic reactions and

9 oxidative status regulation, as well as potentially fine-tuning the Krebs cycle[1,2]. NNT

10 deficiency causes familial glucocorticoid deficiency in humans and type II diabetes-

11 like abnormalities in mice (common strain C57BL/6J has dysfunctional

12 transhydrogenase)[3,4]. The catalytic mechanism was proposed to involve a remarkable

13 ~180° rotation of the entire NADP(H)-binding domain that alternately participates in

14 hydride transfer and proton channel gating but the details of this process remained

15 obscure due to the lack of the high-resolution structures of intact NNT[5,6]. Here we

16 report the first atomic structure of intact mammalian transhydrogenase, solved by

17 cryo-EM in different conformational states. We show how the NADP(H)-binding

18 domain opens the proton channel to the opposite sides of the membrane and provide

19 structures of these two states. We also describe the catalytically important interfaces

20 and linkers between the membrane and the soluble domains and their roles in

21 nucleotide exchange. These structures allow us to propose a revised and detailed

22 mechanism for a unique coupling process in transhydrogenase that is consistent with a

23 large body of previous biochemical work. Results presented here are relevant for the

24 development of currently unavailable NNT inhibitors with therapeutic potential in

25 ischaemia reperfusion injury, metabolic syndrome and some cancers[7–9].

26

**Main text**

Transhydrogenase always exists as a homodimer. Each monomer is composed of
three domains, NAD(H)-binding dI, transmembrane dII and NADP(H)-binding dIII,
split between one, two or three polypeptides (Fig. 1a, Extended Data Fig. 1).
Structures of isolated domains and dI$_2$dIII complexes from several species were
solved in native, reduced or oxidised states, however, they failed to explain the unique
mechanism of NNT which requires coordination of all the domains in the dimer[10–14].
The only intact architecture of NNT was determined at low resolution (6.9 Å) for the
*T. thermophilus* enzyme in the presence of NADP[+5]. It showed that NNT is an
asymmetric dimer, with one dIII being "face-up" (presenting NADP(H) to dI for
hydride transfer) and the other dIII being "face-down" (with NADP(H) site facing
dII) (Fig. 1b)[5]. This led to a proposal of a unique "division of labour" mechanism in
which dIII rotates ~180$^0$ and alternatively functions in proton translocation (face-
down) and hydride transfer (face-up)[6]. While being consistent with the *T.
thermophilus* architecture and most of the previous biochemical work, in the absence
of detailed structural information the mechanism was largely speculative and it failed
to account for the different effects of NADP^{+}/NADPH on the conformation of
NNT[15,16].

To define the mechanism, we solved structures of a stable and active preparation
of ovine NNT at pH 7.4 in the apo, NADP^{+}-bound and NADPH-bound forms at up to
2.9 Å resolution using cryo-EM (Extended Data Fig. 2-4). The only observed 3D
class of particles in the apo-NNT dataset adopted an unexpected and previously
unobserved "double face-down" conformation with both dIII domains tightly attached

51    to dII in the "face-down" orientation (Fig. 1a). In the $NADP^+$ dataset the main class

52    showed a similar conformation, but with improved resolution, possibly due to the

53    stabilising effects of the bound nucleotide (Fig. 1c and 2a, Extended Data Fig. 3 and

54    5). $NADP^+$ dataset also resulted in the structure of the less populated class ("single

55    face-down", Fig. 1b) in which one dIII is detached from dII, $dI_2$ is more tilted and,

56    importantly, the proton channel has different conformations in the two monomers, as

57    discussed below (Extended Data Fig. 6). Excellent EM maps resulted in high quality

58    full atomic models of mammalian NNT (Extended Data Fig. 5-6, Extended Data

59    Table 1). Incubating NNT with NADPH induced global conformational changes, as

60    predicted[15,16], and we did not observe any "double face-down" class (Fig. 2a,

61    Extended Data Fig. 4a). Only ~11 % of particles had one dIII weakly bound to dII and

62    the rest of the particles corresponded to many different "double-detached" classes

63    with both dIII domains detached and tethered only by a dII-dIII linker, which allowed

64    striking tilting of $dI_2$ in all directions (Fig. 2). We conclude that in the mammalian

65    enzyme, $NADP^+$ and NADPH on their own promote dIII detachment to various

66    degrees but do not lead to a stable dI-dIII (face-up) interface formation.

67

68        Some novel features of the structure, such as dI-dII linker, and other additional

69    results are described in the Supplementary Discussion. The mammalian-specific

70    helices TM1 and TM5 form an unexpected extended dII dimer interface, possibly

71    stabilising mammalian NNT (Fig. 3a). The core fold of dII is conserved between *T.*

72    *thermophilus* and ovine. The likely proton translocation pathway, as proposed earlier,

73    is formed by TM3-4, TM9-10, and TM13-14, arranged in a hexagram[5,17,18]. We

74    observed two conformations of the proton channel, depending on the attachment of

75    the dIII domain, which inserts the helix 4 (residues 929-937) and the $NADP^+$-

76    coordinating loop (residues 920-927) deeply between the key TM helices 3, 9 and 13,

77    pushing them apart (Fig. 4a,b). Analysis of the proton channel in the dIII-attached

78    state starting from the N-side (bacterial cytoplasm or mitochondrial matrix) indicates

79    a narrow block followed by a group of conserved polar residues (His664, Asn796 and

80    Asn489), a dry hydrophobic stretch and a cluster of negatively charged residues at the

81    exit, appropriate for proton "gathering" from the P-side in forward reaction (Fig. 3b,c,

82    Extended Data Fig. 6g). Strikingly, secondary structures of helices TM3 and TM9 are

83    distorted around this region, signifying the conformational flexibility needed for the

84    proton translocation (Fig. 3b).

85

86    dIII detachment from dII induces a significant shift of the loops CL6/CL7, helix

87    CL8 and the matrix-facing sides of TM9, 10, 11, 13 and 14 towards the centre of the

88    dII, with up to 3.5 Å displacements (Fig. 4a). This results in a more compact packing

89    of the helices making dIII-detached dII much more similar to the *T. thermophilus* dII

90    (also detached from dIII) than dIII-attached dII (Extended data Fig. 7a,b). With dIII

91    detached, the proton channel adopts a more closed conformation from the P-side

92    (Extended data Fig. 7f,g). Dramatically, H664 flips "down" (towards P-side) and

93    S799 "up", in line with the MD predictions (Fig 4a, Extended Data Fig. 7c)[17]. H664

94    becomes more accessible for protonation from the matrix side, both due to the re-

95    arrangements in the channel and, importantly, the removal of the dIII-NADP(H)

96    "plug", exposing the dII surface to the solvent (Fig. 3). Modelling of water molecules

97    is consistent with this conclusion: in the dIII-attached dII one water molecule is bound

98    above and one below the H664-N489-N796 ring while in the dIII-detached state, the

99    P-side water molecule disappears and the S799 flips "downwards" (Extended Data

100    Fig. 7d). Cryo-EM density of the highly coordinated P-side water molecule is visible

101    in our 2.9 Å map (Extended Data Fig. 7e).

102

103    The conformation of dIII bound to dII differs from crystal structures of isolated

104    dIII at the interface-forming sites and in the nucleotide binding pocket (Fig. 4b,

105    Extended Data Fig. 8a)[10,11,14]. Loop E (residues 1002-1010) is a transhydrogenase-

106    specific element that "occludes" the nucleotide in isolated dIII, preventing its

107    exchange with the solution[10,12]. This loop is displaced by the dII CL7 and has only

108    very weak density in our "double face-down" NADP$^+$ structure, allowing NADP$^+$ to

109    insert deeply into the proton channel. In the apo-NNT structure, loop E is completely

110    disordered allowing free exchange of nucleotide (Extended data Fig. 8b,c). dII

111    binding also induces some opening around the ribose diphosphate, i.e. breaking of the

112    R925-Y890 stacking interactions and the R925 bonds with the diphosphate that have

113    not been observed in any dIII or dI$_2$dIII crystal structures (Fig 4c)[10,12]. In apo-NNT,

114    this opening is even more pronounced with R925 being rotated outwards (Extended

115    Data Fig. 8c). We conclude that the NADP$^+$ molecule is partially occluded in the

116    face-down binding site, but less so than in the detached dIII.

117

118    We can now revise the catalytic mechanism of transhydrogenase, involving dIII

119    flipping as proposed earlier[6], on the basis of our observations and previous functional

120    and mutagenesis results (Extended Data Fig. 9a, Supplementary Tables 1-3),

121    summarised in the following principal considerations.

122

123    It has been well established from previous work that: a) dI remains open to

124    nucleotide exchange throughout the reaction cycle as confirmed by high rates of

125  binding of NAD(H) to dI during the catalytic cycle[19,20]. b) The dI-dIII interface is

126  transient, hydride transfer is fast and does not limit the reaction[21]. c) When dIII is

127  detached, bound NADP(H) is occluded, as shown by decreased $K_d$ for NADP(H) in

128  isolated dIII ($\sim 10^{-9}$ M) compared to intact enzyme ($\sim 10^{-6}$ M), copurification of bound

129  nucleotide with isolated dIII and well-ordered and closed loop E in dIII

130  structures[10,12,22,23]. H664 and R544 mutations which lead to dIII detachment also lead

131  to co-purification with NADP(H)[18,24].

132

133     The following principle was speculatively proposed earlier[6] and is now validated

134  by our structures: d) The formation of the dII-dIII interface is necessary for nucleotide

135  exchange, as shown by our structures demonstrating loop E opening (Extended Data

136  Fig. 8). It is further validated by R544 mutants which disrupt the dII-dIII interface[24].

137

138     Crucial new insights from the structural data presented here are: e) Apo-dIII is

139  attached to dII and can detach only when bound to NADP(H) (Fig. 2a). f) The proton

140  channel is open only to the N-side when dIII is detached and only to the P-side when

141  dIII is attached (Fig. 4, Extended Data Fig. 7). g) The dIII-NADP(H) detachment

142  from dII depends on the protonation state of the key histidine in the proton channel

143  (H664 in ovine). dIII-NADP$^+$ is detached from protonated H664$^+$ but is attached to

144  the neutral H664. Vice versa, dIII-NADPH is detached from H664 and is attached to

145  H664$^+$. In other words, dIII-NADP(H) attachment modifies H664 $pK_a$: bound

146  NADPH promotes its protonation and NADP$^+$ de-protonation. This pattern is

147  consistent with the direct electrostatic interaction between H664 and the charged

148  nicotinamide ring (positive in NADP$^+$ and negative in NADPH) separated only by

149  about 13 Å (Fig. 3e), much closer than 19 Å predicted previously[5]. The $pK_a$ of His664

150 was experimentally estimated to be ~5.5[25], which is consistent with PROPKA

151 calculations on our structures (suggesting $pK_a$ ~5). Since our datasets were collected

152 at pH 7.4, when H664 is mostly de-protonated, we observed mostly attached dIII-

153 $NADP^+$ and mostly detached dIII-NADPH, consistent with this proposal. dIII

154 detachment from dII in the presence of $NADP^+$ and $H664^+$ is also validated by low

155 pH-stimulation of $NADP^+$-dependent cyclic reaction (hydride transfer from NADH to

156 $NAD^+$ via occluded $NADP^+$)[25,26]. Cyclic reaction cannot inform us on specific

157 NADPH effects as the main species in the NADPH-initiated cycle is still the occluded

158 dIII-$NADP^{+}$[26]. However, NADPH-stimulated dIII detachment at neutral-high pH has

159 been demonstrated experimentally by stimulated trypsinolysis in the presence of

160 NADPH (but not $NADH/NAD^+$)[15]. We analysed the full pH dependence of

161 trypsinolysis in the presence of all substrates and showed that NADPH stimulates

162 trypsinolysis with increasing pH, while $NADP^+$ stimulates it with decreasing pH

163 (Extended Data Fig. 2e), validating the predicted H664-NADP(H) interactions.

164

165   On the basis of these principles we propose a robust and elegant mechanism

166 which explains the full reversibility of NNT, pH dependencies of reverse and cyclic

167 reactions, effects of $NADP^+$ and NADPH on the NNT conformation and is validated

168 by the phenotypes of various mutants, particularly within the proton translocation

169 pathway, E loop and dII-dIII interface (Fig. 5, Supplementary Video 1). Proton

170 translocation and nucleotide exchange are tightly coupled by direct interactions

171 between H664 and NADP(H): attachment/detachment of NADP(H)-bound dIII is

172 strictly dependent on the protonation state of H664 and opens the proton channel to

173 the opposite sides of the membrane. "Slipping", or uncoupling, is prevented because

174 proton translocation cannot happen without nucleotide exchange. The forward

175   reaction occurs under conditions with high pmf and excess of NADP$^+$. With dIII

176   detached, H664 is unprotonated as it is exposed to the matrix with its relatively high

177   pH (step 1, Fig. 5). After hydride transfer, dIII-NADPH swivels down and attaches to

178   dII-H664, opening it to the P-side (step 2). This allows H664 protonation from the P-

179   side, where pH is lower (and His pK$_a$ is shifted higher due to interaction with

180   NADPH). Nucleotide exchange follows, due to NADP$^+$ excess and opened dIII (step

181   3). dIII-NADP$^+$ detaches from dII-H664$^+$, which opens dII to the N-side where H664$^+$

182   is de-protonated (step 4). dIII-NADP$^+$ associates with dI, allowing for hydride transfer

183   (back to step 1). All the steps can be easily reversed in the appropriate conditions

184   (high NADPH and low pmf), giving rise to the reverse reaction (Extended Data Fig.

185   9b, Supplementary Discussion).

186

187   This mechanism implies anti-phase action of two monomers, or "division of

188   labour" as suggested previously[6], which is absolutely necessary for bacterial enzymes

189   without dI-dII linker, where one dIII has to be attached to dI$_2$ at all times to prevent

190   the loss of dI$_2$. Mammalian NNT also demonstrates half-of-sites inhibition,

191   catalytically inactive monomeric dI and negative cooperativity of NAD(H) and

192   NADP(H) sites between monomers, strongly suggesting anti-phase mechanism[27–29].

193   The presence of dI-dII linker could make a strict anti-phase action less of a

194   requirement for the mammalian enzyme, but such action would avoid steric clashes

195   between independently functioning dIIIs and the swivelling "up" of one dIII is the

196   best explanation for the initiation of the detachment, after hydride transfer, of the

197   other dIII from dI$_2$. The dI-dII linker could also contribute towards higher efficiency

198   of the mammalian enzyme, as the dI-dIII interface can be weaker and allow for faster

199   turnover. Biochemical data confirms that dI-dIII interaction in bacteria is much

200 stronger than in mammals[20,30]. The existence of a unique auto-inhibited "double face-

201 down" conformation in mammalian NNT could be important for its additional

202 regulation. Further data will be required to determine the significance of the anti-

203 phase action in NNT as well as to test all the implications of the proposed mechanism.

204

205 **References**

206 1.     Jackson, J. B. A review of the binding-change mechanism for proton-

207       translocating transhydrogenase. *Biochim. Biophys. Acta - Bioenerg.* **1817**,

208       1839–1846 (2012).

209 2.     Sazanov, L. A. & Jackson, J. B. Proton-translocating transhydrogenase and

210       NAD- and NADP-linked isocitrate dehydrogenases operate in a substrate cycle

211       which contributes to fine regulation of the tricarboxylic acid cycle activity in

212       mitochondria. *FEBS Lett.* **344**, 109–116 (1994).

213 3.     Meimaridou, E. *et al.* Mutations in NNT encoding nicotinamide nucleotide

214       transhydrogenase cause familial glucocorticoid deficiency. *Nat. Genet.* **44**,

215       740–2 (2012).

216 4.     Toye, A. A. *et al.* A genetic and physiological study of impaired glucose

217       homeostasis control in C57BL/6J mice. *Diabetologia* **48**, 675–686 (2005).

218 5.     Leung, J. H. *et al.* Structural biology. Division of labor in transhydrogenase by

219       alternating proton translocation and hydride transfer. *Science* **347**, 178–81

220       (2015).

221 6.     Jackson, J. B., Leung, J. H., Stout, C. D., Schurig-Briccio, L. A. & Gennis, R.

222       B. Review and Hypothesis. New insights into the reaction mechanism of

223       transhydrogenase: Swivelling the dIII component may gate the proton channel.

224       *FEBS Letters* **589**, 2027–2033 (2015).

225 7.     Li, S. *et al.* Nicotinamide nucleotide transhydrogenase-mediated redox

226       homeostasis promotes tumor growth and metastasis in gastric cancer. *Redox*

227       *Biol.* **18**, 246–255 (2018).

228 8.     Santos, L. R. B. *et al.* NNT reverse mode of operation mediates glucose control

229       of mitochondrial NADPH and glutathione redox state in mouse pancreatic β-

230     cells. *Mol. Metab.* **6**, 535–547 (2017).

231  9.  Nickel, A. G. *et al.* Reversal of Mitochondrial Transhydrogenase Causes

232     Oxidative Stress in Heart Failure. *Cell Metab.* **22**, 472–484 (2015).

233  10.  Prasad, G. S., Sridhar, V., Yamaguchi, M., Hatefi, Y. & Stout, C. D. Crystal

234     structure of transhydrogenase domain III at 1.2 A resolution. *Nat. Struct. Biol.*

235     **6**, 1126–31 (1999).

236  11.  Cotton, N. P. J., White, S. A., Peake, S. J., Mcsweeney, S. & Jackson, J. B. The

237     Crystal Structure of an Asymmetric Complex of the Two Nucleotide Binding

238     Components of Proton-Translocating Transhydrogenase. *Structure* **9**, 165–176

239     (2001).

240  12.  Sundaresan, V., Yamaguchi, M., Chartron, J. & Stout, C. D. Conformational

241     Change in the NADP(H) Binding Domain of Transhydrogenase Defines Four

242     States. *Biochemistry* **42**, 12143–12153 (2003).

243  13.  Johansson, T. *et al.* X-ray structure of domain I of the proton-pumping

244     membrane protein transhydrogenase from *Escherichia coli. J. Mol. Biol.* **352**,

245     299–312 (2005).

246  14.  Mather, O. C., Singh, A., Van Boxel, G. I., White, S. A. & Jackson, J. B.

247     Active-site conformational changes associated with hydride transfer in proton-

248     translocating transhydrogenase. *Biochemistry* **43**, 10952–10964 (2004).

249  15.  Yamaguchi, M., Wakabayashi, S. & Hatefi, Y. Mitochondrial Energy-Linked

250     Nicotinamide Nucleotide Transhydrogenase: Effect of Substrates on the

251     Sensitivity of the Enzyme to Trypsin and Identification of Tryptic Cleavage

252     Sites. *Biochemistry* **29**, 4136–4143 (1990).

253  16.  Yamaguchi, M. & Hatefi, Y. Mitochondrial nicotinamide nucleotide

254     transhydrogenase: NADPH binding increases and NADP binding decreases the

255        acidity and susceptibility to modification of cysteine-893. *Biochemistry* **28**,

256        6050–6 (1989).

257  17.  Padayatti, P. S. *et al.* Critical Role of Water Molecules in Proton Translocation

258        by the Membrane-Bound Transhydrogenase. *Structure* 1–9 (2017).

259  18.  Glavas, N. A., Hou, C. & Bragg, P. D. Involvement of Histidine-91 of the β

260        Subunit in Proton Translocation by the Pyridine Nucleotide Transhydrogenase

261        of *Escherichia coli. Biochemistry* **34**, 7694–7702 (1995).

262  19.  Venning, J. D., Peake, S. J., Quirk, P. G. & Jackson, J. B. Stopped-flow

263        reaction kinetics of recombinant components of proton-translocating

264        transhydrogenase with physiological nucleotides. *J. Biol. Chem.* **275**, 19490–7

265        (2000).

266  20.  Yamaguchi, M. & Hatefi, Y. High cyclic transhydrogenase activity catalyzed

267        by expressed and reconstituted nucleotide-binding domains of *Rhodospirillum*

268        *rubrum* transhydrogenase. *Biochim. Biophys. Acta - Bioenerg.* **1318**, 225–234

269        (1997).

270  21.  Venning, J. D., Bizouarn, T., Cotton, N. P. J., Quirk, P. G. & Jackson, J. B.

271        Stopped-flow kinetics of hydride transfer between nucleotides by recombinant

272        domains of proton-translocating transhydrogenase. *Eur. J. Biochem.* **257**, 202–

273        209 (1998).

274  22.  Fjellström, O., Johansson, C. & Rydström, J. Structural and catalytic properties

275        of the expressed and purified NAD(H)- and NADP(H)-binding domains of

276        proton-pumping transhydrogenase from *Escherichia coli. Biochemistry* **36**,

277        11331–11341 (1997).

278  23.  Bizouarn, T., Van Boxel, G. I., Bhakta, T. & Jackson, J. B. Nucleotide binding

279        affinities of the intact proton-translocating transhydrogenase from *Escherichia*

280      *coli. Biochim. Biophys. Acta - Bioenerg.* **1708**, 404–410 (2005).

281    24.    Glavas, N. A. & Bragg, P. D. The mechanism of hydride transfer between

282      NADH and 3-acetylpyridine adenine dinucleotide by the pyridine nucleotide

283      transhydrogenase of *Escherichia coli. Biochim. Biophys. Acta* **1231**, 297–303

284      (1995).

285    25.    Sazanov, L. A. & Jackson, J. B. Cyclic reactions catalysed by detergent-

286      dispersed and reconstituted transhydrogenase from beef-heart mitochondria;

287      implications for the mechanism of proton translocation. *Biochim. Biophys. Acta*

288      **1231**, 304–312 (1995).

289    26.    Hutton, M., Day, J. M., Bizouarn, T. & Jackson, J. B. Kinetic resolution of the

290      reaction catalysed by proton-translocating transhydrogenase from *Escherichia*

291      *coli* as revealed by experiments with analogues of the nucleotide substrates.

292      *Eur. J. Biochem.* **219**, 1041–1051 (1994).

293    27.    Phelps, D. C. & Hatefi, Y. Interaction of purified nicotinamidenucleotide

294      transhydrogenase with dicyclohexylcarbodiimide. *Biochemistry* **23**, 4475–4480

295      (1984).

296    28.    Yamaguchi, M. & Hatefi, Y. Energy-transducing nicotinamide nucleotide

297      transhydrogenase. Nucleotide binding properties of the purified enzyme and

298      proteolytic fragments. *J. Biol. Chem.* **268**, 17871–17877 (1993).

299    29.    Obiozo, U. M. *et al.* Substitution of tyrosine 146 in the dI component of

300      proton-translocating transhydrogenase leads to reversible dissociation of the

301      active dimer into inactive monomers. *J. Biol. Chem.* **282**, 36434–36443 (2007).

302    30.    Fjellstrom, O. *et al.* Catalytic Properties of Hybrid Complexes of the NAD(H)-

303      Binding and NADP(H)-Binding Domains of the Proton-Translocating

304      Transhydrogenases from *Escherichia coli* and *Rhodospirillum rubrum*.

305       *Biochemistry.* **38**, 415–422 (1999).

306

307

308    **Main Figure Legends**

309    **Figure 1. Mammalian transhydrogenase.**

310    **a**, Schematic representation of the domains, linkers, binding sites and conformation
311    of the mammalian transhydrogenase in the "double face-down" (both dIII attached to
312    dII) conformation (apo and NADP$^+$ datasets). **b**, Other conformations of NNT present
313    in our datasets (one or both dIII detached in the presence of NADP$^+$ and NADPH),
314    the asymmetric conformation in *T. thermophilus* (N.B. the absence of dI-dII linker)
315    and the sterically prohibited double-face-up conformation. **c**, The cryo-EM density of
316    transhydrogenase in the "double face-down" NADP$^+$ state, with two monomers
317    coloured differently. **d**, Atomic model of mammalian NNT with domains coloured as
318    in panel a, and mammalian-specific elements dI-dII linker, TM1 and TM5 highlighted
319    in blue. Bound nucleotides are shown in black.

320

321    **Figure 2. NADP(H) binding influences the overall conformation of**
322    **transhyrogenase.**

323    **a**, Structures and relative abundancies of different conformations of NNT observed in
324    the datasets. "Double face-down" conformation was the only form observed in apo-
325    NNT and the major form in the NADP$^+$ datasets, "single face-down" or "one dIII-
326    detached" conformation was a minor form in NADP$^+$ and NADPH datasets and
327    "double dIII-detached" was a major form in NADPH dataset. **b**, NNT-NADPH
328    particles were analysed using multibody refinement in RELION 3.0 using dI$_2$ and dII$_2$
329    masks which revealed a high degree of tilting of dI$_2$ domain in all directions,
330    consistent with both dIII being dissociated from the rest of the particle and disrupting
331    the overall solidity of the enzyme. Two bins of particles from the extreme ends of the
332    distribution along two principal components are aligned by dII$_2$ and the difference in
333    dI$_2$ tilt is depicted in different shades of yellow and green.

334

335

**Figure 3. The transmembrane dII domain and the proton translocation pathway in the "double face-down" conformation.**

**a**, Organisation of transmembrane helices in the NNT dimer. The monomer on the left is coloured blue-to-red from N- to C-terminus and the monomer on the right has the inner proton channel-lining TM helices highlighted in magenta and the outer scaffolding helices in pink. The dimer interface consisting of eight helices is significantly larger than the four-helix interface of *T. thermophilus*. **b**, Conserved residues of the proton transfer pathway. Dowser-predicted water molecules are shown as red spheres. The distorted α-helical area is indicated as $3_{10}$ helix. **c**, Proton translocating pore features a narrow block close to the matrix (N) side and a dry stretch in the middle of the membrane. Four of the predicted water molecules lie within the central pore. **d**, Detailed view of the matrix proton entry site with conserved residues and hydrogen bonding network shown. **e**, Nicotinamide ring is bound 13 Å away from H664 allowing for electrostatic interactions.

**Figure 4. dIII attachment changes the conformation of the proton translocation pathway and opens the NADP(H)-binding pocket.**

**a**, Comparison of dII in dIII-associated (cyan) and dissociated (green) states from "single face-down" structure. dIII dissociation results in the tilting of TM helices towards the central axis. Expanded views show rearrangement of the N-side proton entry side in dII. Notably, H664 and S799 flip and the surrounding N489 and N796 change conformations significantly, opening the channel to the N-side when dIII is detached. **b**, The interface between dIII and dII. Helix 4 and loop D, which are conserved transhydrogenase-specific elements flanking the central Rossmann fold, form extensive contacts with the cytoplasmic loops of the dII. Loop E is displaced by dII binding. **c**, NADP(H) binding pocket comparison between ovine dIII-dII and human dIII-NADP$^+$ (PDB 1djl, in grey) reveals breaking of R925 interactions with diphosphate and Y890.

365 **Figure 5. The catalytic mechanism of transhydrogenase**

366 NNT always works as a dimer. Key steps in the mechanism for the monomer in

367 colour are described in the main text. The other monomer (grey) works in the anti-

368 phase fashion. Nucleotide in dIII exists in either occluded (full line) or open state

369 (dashed line). Key check-point in the mechanism is that proton translocation across

370 the membrane cannot proceed to completion without nucleotide exchange in step 3.

371 The dIII-NADP(H) and dII-H664 interactions, ensuring this coupled reaction, can be

372 summarised as follows, with (*) meaning strong interaction and ($\leftarrow\rightarrow$) weak

373 interaction or repulsion:

374 $NADP^+ * H \quad NADP^+ \leftarrow\rightarrow H^+$

375 $NADPH * H^+ \quad NADPH \leftarrow\rightarrow H$
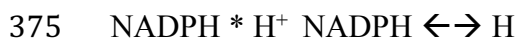
376

377      **Methods**

378      <u>Purification of transhydrogenase from ovine mitochondria</u>

379      All the described procedures were done at 4°C. Mitochondria were purified from

380      fresh ovine heart tissue by differential centrifugation and stored at −80°C according to

381      the Procedure 3 by Smith[31]. On the day of purification, inner mitochondrial

382      membranes were isolated as described for the respiratory complex I purification[32].

383      Briefly, 10 g of mitochondria were ruptured by homogenisation in 100 mL milliQ

384      water, membranes were separated by 45 min centrifugation at 50000 g and

385      resuspended in 100 mL of buffer M (20 mM HEPES, pH 7.4, 40 mM NaCl, 1 mM

386      EDTA, 10% v/v glycerol, 2 mM DTT and 0.002% PMSF). After another round of

387      resuspension and centrifugation, membranes were resuspended in 50 mL of buffer M.

388      LMNG (10 %) was added dropwise to this suspension to 1 % and after stirring for 45

389      min, the sample was centrifuged at 50000 g for 45 minutes. The supernatant was

390      filtered with a 0.22 μm filter and loaded onto a 45 mL Q-sepharose HP anion

391      exchange column equilibrated in buffer Q-A (20 mM HEPES pH7.4, 40 mM NaCl, 2

392      mM EDTA, 10% v/v glycerol, 1 mM DTT, 0.05% LMNG). Proteins were eluted with

393      a 400 mL linear gradient with 0-17% Q-B buffer (Q-A buffer with 1 M NaCl). NNT

394      eluted as a broad peak around 110 mM NaCl and fractions containing significant

395      amounts of NNT based on the activity assay and the SDS-PAGE profile were pooled

396      and dialysed overnight against a 10-fold volume excess of buffer D (20 mM MES, pH

397      5.8, 2 mM EDTA, 10% v/v glycerol, 1 mM DTT, 0.01% LMNG). This lowered the

398      pH and conductance of the sample below 6 and 2 mS/cm, respectively, and made it

399      suitable for loading onto a 45 mL SP-Sepharose HP cation exchange column

400      equilibrated in buffer SP-A (20 mM MES pH5.8, 10 mM NaCl, 2 mM EDTA, 10%

401      v/v glycerol, 1 mM DTT, 0.025% LMNG). Elution with a 100 mL 0-20% linear

402     gradient with buffer SP-B (SP-A with 1 M NaCl) gave a sharp elution peak of

403     relatively pure NNT at around 35 mM NaCl (conductance 4 mS/cm). Fractions

404     containing NNT were concentrated to 4 mg/mL using a 100 kDa cut-off concentrator

405     and stored at 30% glycerol under liquid nitrogen. On the day of a cryo-EM grid

406     preparation, a sample of NNT was thawed on ice and loaded onto a Superose 12

407     10/300 gel filtration column equilibrated in buffer GF (20 mM HEPES, pH 7.4, 50

408     mM NaCl, 1 mM EDTA, 0.002% LMNG) to remove excess detergent and remaining

409     protein contaminants. The purest and the most concentrated fractions of NNT eluted

410     at ~10.5 mL and were concentrated to 5 mg/mL using a Millipore 100-kDa cut-off

411     filter and used immediately for cryo-EM grid preparation (Extended Data Fig. 2). In

412     some purifications, 0.002% LMNG in GF buffer was substituted by 0.05% FOM,

413     which gave a monodisperse and highly active NNT but grids suitable for cryo-EM

414     data collection could not be prepared from FOM preparations as the protein started to

415     aggregate on the grid at concentrations higher than 2 mg/mL. Apo form of our

416     preparation lacked any bound nucleotide, as confirmed by the absence of cyclic

417     reaction without the addition of exogenous $NADP^+$ (data not shown).

418

419     <u>Electron microscopy</u>

420     0.05% CHAPS was added to the protein sample before grid preparation to improve

421     the ice quality and the particle distribution. Substrates at 5 mM concentration were

422     added to the protein 15-30 min before the grid preparation and the samples were

423     incubated on ice. 2.7 μL protein sample was applied to a freshly glow-discharged

424     Quantifoil 0.6/1 copper grid and blotted for 4-6 s using a blotting force of 25 at 4°C

425     and 100% humidity in an FEI Vitrobot Mark IV. Grids were flash-frozen in liquid

426     ethane and stored in liquid nitrogen until data-collection. $NNT-NADP^+$ grids were

427    imaged using a 300 kV Titan Krios electron microscope equipped with a Gatan

428    energy filtered K2 summit camera with a slit width of 20 eV at The Astbury Centre

429    for Structural Molecular Biology of the University of Leeds. NNT-NADPH grids

430    were imaged using a 300 kV Titan Krios electron microscope equipped with a Gatan

431    energy filtered K2 summit camera with a slit width of 20 eV at the CM01 beamline,

432    ESRF, Grenoble. Images were collected with EPU in a K2 super-resolution mode

433    with a nominal magnification of 130000x and a physical pixel size of 1.065 Å for

434    NNT-NADP$^+$ and 1.07 Å for NNT-NADPH dataset. Total dose of 72 e/Å$^2$ (NNT-

435    NADP$^+$) or 70 e/Å$^2$ (NNT-NADPH) was fractionated into 40 frames of 250 ms each.

436    Apo-NNT grids were imaged using a 300 kV Titan Krios electron microscope

437    equipped with a Gatan energy filtered K3 camera with a slit width of 20 eV at the

438    Institute of Science and Technology Austria. Physical pixel size was 0.84 Å and the

439    total dose of 90 e/Å$^2$ was fractionated into 88 frames of 36 ms each.

440

441    <u>Image processing</u>

442    We collected 2272 movies for the NADP$^+$ dataset, 1722 movies for NADPH dataset

443    and 786 movies for the apo-NNT dataset. The processing was done in RELION 2.1[33]

444    unless otherwise stated. Movie frames were aligned using MotionCor2[34] and initial

445    CTF parameters were estimated from averaged images using CTFFIND[35].

446    Autopicking with 2D class averages as references resulted in 516395 particles for the

447    NADPH dataset, 1076677 particles for the NADP$^+$ dataset and 500001 particles for

448    the apo dataset. Multiple rounds of 2D classification and 3D classification were

449    performed to classify considerably heterogeneous particles in both datasets (Extended

450    data Fig. 3,4). CTF parameters and per-particle trajectories in the best two classes

451     from the $NADP^+$ dataset were estimated and corrected (particle polishing) using

452     RELION 3.0[36]. Local resolution was estimated using Resmap 5.0[37].

453

454     For the $NADP^+$ dataset we performed one round of 2D classification followed by two

455     rounds of 3D classification with 3x and 2x binned particles, respectively, which

456     resulted in eight classes containing 342284 particles from which it was obvious that

457     there is a considerable heterogeneity in the conformations of $dI_2$ and dIIIb. To address

458     this, the particles were re-extracted without binning and refined with a $dII_2dIII_2$ mask

459     to 3.5 Å and then classified into ten classes without searches and without a mask to

460     separate the particles based on the relative position of the $dI_2$. By combining similar

461     classes and auto-refining them, we separated six different states of NNT which differ

462     from each other with respect to the positions of $dI_2$ and dIIIb. Two of these classes

463     were resolved to 13 Å, further two to 7 Å and the best two classes to 3.7 and 3.2 Å.

464     From the latter two maps it was obvious that the density for $dI_2$ was still weaker than

465     for the rest of the particle, indicating remaining heterogeneity in the positions of $dI_2$,

466     hence the final maps for these two classes were produced by combining focus-refined

467     maps of $dII_2dIII_2$ and $dI_2$ parts. This gave the final map for class 1 (closed) with 2.9 Å

468     resolution in the $dII_2dIII_2$ and 3.2 Å resolution in the $dI_2$ and for class 2 (open) 3.5 Å

469     resolution for the $dII_2dIII$ and 4.1 Å resolution for the $dI_2$. Due to the poor quality of

470     the map for the open class in some regions of dIIb (CL6,7,8), we hypothesised that

471     there is still remaining conformational heterogeneity present in this class and we

472     performed another round of classification of these particles with a mask around dIIb

473     to sort out any particles with dIIIb attached/semi-attached to dII. This procedure

474     removed 52% particles and we performed an auto-refinement with a $dII_2dIII$ mask of

475     the remaining 28498 particles with dIIIb unambiguously detached. This resulted in a

476  3.7 Å map with dIIb density much better resolved and clearly different from the

477  density of dIIa (which has dIII attached) and was used for model building.

478

479  For the NADPH dataset, we performed one round of 2D classification followed by

480  one round of 3D classification on 510073 3x binned particles with the same

481  parameters as in the $NADP^+$ dataset, which failed to yield any class with visible

482  secondary structural features. We performed extensive classifications of these

483  particles into 4-20 classes with T values between 4 and 12 and different filtering of

484  the reference volumes which all failed to give a single well-defined class with

485  secondary structural features. Nevertheless, we selected 405141 particles from the

486  best 4 classes from a classification with T=8 and k=6 (same as for $NADP^+$ dataset) for

487  further classification attempts. Another round of extensive classifications was

488  performed on this particle stack with the best results obtained from a T=8, k=20 run.

489  Even in this run only ~6 classes had well-defined features corresponding to the

490  domains of NNT. These 6 classes were re-extracted and refined which gave structures

491  at 8.3, 9.2, 13, 16, 16, and 16 Å and revealed a high degree of $dI_2$ and dIII mobility

492  (Extended Data Fig. 4a). To address this, we tried to refine the 405141 particles

493  together into one consensus structure at 13 Å, followed by focused refinement of

494  either $dI_2$ or $dII_2$ but neither of these strategies yielded structures better than 9 Å,

495  probably due to the too large conformational heterogeneity within the consensus

496  refinement. Furthermore, $dI_2$ and $dII_2$ are only 80 kDa each and $dII_2$ is obscured by a

497  micelle which further complicates the alignment of such a heterogeneous dataset.

498  Finally, we performed multi-body refinement in RELION 3.0 starting from the

499  consensus refinement of 405141 particles and using masks for the two bodies: $dI_2$ and

500  $dII_2$. This yielded a 9 Å reconstruction of $dI_2$ and 10 Å reconstruction of $dII_2$ but more

501 importantly, the principal component analysis showed the striking degree of $dI_2$

502 mobility in these particles (Fig. 2de). This is not unexpected as upon dIII dissociation,

503 $dI_2$ remains only loosely tethered to the rest of the particle by a flexible dI-dII linker.

504

505 The apo-NNT dataset was fully processed in RELION 3.0. We manually selected 643

506 good images and extracted 3x binned particles. Only one conformation of NNT could

507 be observed using various 3D classification schemes, hence the 283706 particles

508 corresponding to it were extracted without binning and auto-refined to 4.5 Å. From

509 this structure it was clear that $dI_2$ exhibits the same heterogeneity as in the $NADP^+$

510 dataset. To improve the resolution in the dII-dIII, we focus-refined around this region

511 and classified the particles without searches into 6 classes. The best class with 67908

512 particles was auto-refined and polished to reach the resolution of 3.7 Å. Further

513 polishing or subclassification of this class did not improve the resolution further.

514 Attempts at focus-refinement of $dI_2$ did not improve its resolution compared to the

515 polished full structure of the final selected particles in which local resolution in $dI_2$

516 was ~5 Å. We conclude that $dI_2$ without bound nucleotide exhibits even more

517 disorder than when $NAD^+$ is bound, possibly allowing NAD(H) exchange and $dI_2$

518 binding/release.

519

520 <u>Model building and refinement</u>

521 The initial model was built into the "double face-down" $NADP^+$ class density by

522 starting with the bovine dIII crystal structure with substituted ovine sequence and the

523 dI homology model that was generated using Phyre2 server[38]. dII model and the

524 linkers were built manually in *Coot*[39]. Manually adjusted models were refined using

525 *PHENIX* software[40] using an adapted method for refining cryo-EM structures which

526 uses two rounds of a single cycle of group ADP refinement followed by three cycles

527 of global minimization. This allows optimization of B-factors so that electron

528 radiation-damaged carboxylate side-chains acquire high B-factors and do not lead to

529 main-chain distortions (Letts et al, 2019, in press). The final model for NNT is of very

530 high quality in terms of geometry and fit to density (Supplementary Table 1).

531 Densities for several lipid molecules were observed in each of the half-closed cavities

532 formed by helices TM1, TM2 and TM6 (Extended Data Fig. 5g, 6g-h). They were

533 modelled in the structure as phosphatidylcholines based on their density appearance

534 and the fact that only phosphatidylcholine could reactivate lipid-depleted insect

535 NNT[41].

536 A density corresponding to the adenylate part of $NAD^+$ was observed in the NAD(H)

537 binding site of the dI (Extended Data Fig. 5j,k). We propose that this density is $NAD^+$

538 which remained bound to the enzyme during purification or, more likely, was

539 introduced into the sample as a contaminant from the $NADP^+$ solution. Our $NADP^+$

540 was only 98% pure and at 2% $NAD^+$ contamination, $NAD^+$ concentration would be

541 100 μM which is in the range of the $K_d$ for the enzyme[23,28]. The latter is supported by

542 the fact that in our structure the conserved R139 is in the same extended conformation

543 as in the *E. coli* $dI_2$ with bound $NAD^+$ and differs significantly from the apo or

544 NADH-bound forms[13]. Nevertheless, our structure is a bona fide oxidised ground

545 state conformation of NNT and earlier biochemical work suggests that nucleotide

546 exchange in dI subunit can happen during any stage of the catalytic cycle and does not

547 influence the global conformation of the enzyme[15,16,42,43]. Models for the "single face-

548 down" $NADP^+$ class and the apo NNT were based on the "double face-down" NNT as

549 the starting model. For apo NNT, due to the lack of reliable amino acid side chain

550  information in the cryo-EM density of dI domain, dI was modelled as a polyalanine

551  model based on the 6QTI dI and fit into the density as a rigid body.

552  <u>Structure analysis and preparation of figures</u>

553  Evolutionary conservation scores were projected onto the transhydrogenase structure

554  using ConSurf[44] (Extended Data Fig. 1b). Buried water molecules were modelled

555  using the original Dowser software (Fig. 3, Extended Data Fig. 7)[45]. Proton

556  translocation pore was predicted and analysed using a MOLEonline server[46].

557  Interdomain contacts and binding energy of nucleotides were analysed using the PISA

558  server[47,48]. Models were evaluated using MolProbity and EMRinger[49,50]. Clustal

559  Omega was used for sequence alignment[51,52]. Models and density maps were

560  visualised for analysis and figure preparation purposes in PyMOL 2.2.3 and UCSF

561  Chimera[53].

562  <u>Activity measurements and trypsinolysis</u>

563  Reverse transhydrogenation activity was measured at 30°C spectrophotometrically by

564  following the APAD$^+$ (3-acetylpyridine adenine dinucleotide; NAD$^+$ analogue; $\varepsilon$ =

565  5.1 mM$^{-1}$ cm$^{-1}$) reduction at 375 nm using a Shimadzu UV-2600 UV-VIS

566  spectrophotometer. Background absorption at 455 nm was subtracted from absorption

567  at 375 nm. Reaction buffer was similar to the minimal EDTA-containing buffer used

568  before (20 mM Tris-HCl, pH 6.8, 50 mM NaCl, 0.5 mM EDTA, 0.1% CHAPS, 0.25

569  mg/mL lipids, 100 μM NADPH and 100 μM APAD$^+$)[25]. For lipids we used soybean

570  asolectin or DOPC:CL 4:1 mixture with similar results. Reaction was started with the

571  addition of NNT. Activity depended on the type of detergent used during the final size

572  exclusion chromatography step. Preparations in FOM gave slightly higher activity

573   (~20 U/mg) than in LMNG (~15 U/mg). These values compare favourably to

574   previous measurements[25,54].

575   Trypsinolysis was performed as described previously with a few changes[15]. NNT at

576   0.05 mg/ml in GF buffer with 1 mM HEPES pH 7.4 was incubated with 0.4 mM

577   nucleotides, trypsin (at different mass ratios) and 60 mM BAT buffer (1:1:1 Bis-Tris,

578   acetate, tricine) at pH 5-8. Due to the pH optimum of trypsin being ~8, mass ratio

579   between 1:400 and 1:40 and incubation times between 30 and 60 min were used at

580   different pH values to achieve comparable rates of proteolysis.

581   Proteoliposome reconstitution

582   NNT was reconstituted into proteoliposomes using a detergent dilution procedure as

583   described before[25]. Briefly, NNT purified in FOM or in LMNG was mixed with a

584   500-fold excess of DOPC solubilised in 1% CHAPS. Following a 10 min incubation

585   on ice, the solution was diluted 100-fold and incubated on ice for 3-5 hours before

586   measuring the activities. Reaction was started by substrate additions (NADPH and

587   APAD$^+$ at 100 µM). CCCP (10 µM) was added after 1 min to decouple the proton

588   gradient across proteoliposomes to assess the dependence of the transhydrogenation

589   reaction on the proton motive force. After another 1 min, CHAPS (0.05%) was added

590   to solubilise proteoliposomes and give a total decoupled reverse transhydrogenation

591   activity of both inward and outward facing transhydrogenases.

592

**References**

31. Smith, A. L. [13] Preparation, properties, and conditions for assay of mitochondria: Slaughterhouse material, small-scale. *Methods Enzymol.* **10**, 81–86 (1967).

32. Letts, J. A., Degliesposti, G., Fiedorczuk, K., Skehel, M. & Sazanov, L. A. Purification of ovine respiratory complex I results in a highly active and stable preparation. *J. Biol. Chem.* **291**, 24657–24675 (2016).

33. Scheres, S. H. W. RELION: Implementation of a Bayesian approach to cryo-EM structure determination. *J. Struct. Biol.* **180**, 519–530 (2012).

34. Zheng, S. Q. *et al.* MotionCor2: anisotropic correction of beam-induced motion for improved cryo-electron microscopy. *Nat. Methods* **14**, 331–332 (2017).

35. Rohou, A. & Grigorieff, N. CTFFIND4: Fast and accurate defocus estimation from electron micrographs. *J. Struct. Biol.* **192**, 216–221 (2015).

36. Zivanov, J. *et al.* New tools for automated high-resolution cryo-EM structure determination in RELION-3. *Elife* **7**, (2018).

37. Kucukelbir, A., Sigworth, F. J. & Tagare, H. D. Quantifying the local resolution of cryo-EM density maps. *Nat. Methods* **11**, 63–65 (2014).

38. Kelley, L. A., Mezulis, S., Yates, C. M., Wass, M. N. & Sternberg, M. J. E. The Phyre2 web portal for protein modeling, prediction and analysis. *Nat. Protoc.* **10**, 845–58 (2015).

39. Emsley, P., Lohkamp, B., Scott, W. G. & Cowtan, K. Features and development of Coot. *Acta Crystallogr. D. Biol. Crystallogr.* **66**, 486–501 (2010).

40. Adams, P. D. *et al. PHENIX* : a comprehensive Python-based system for macromolecular structure solution. *Acta Crystallogr. Sect. D Biol. Crystallogr.*

619     **66**, 213–221 (2010).

620     41.     Vandock, K. P., Emerson, D. J., McLendon, K. E. & Rassman, A. A.

621             Phospholipid Dependence of the Reversible, Energy-Linked, Mitochondrial

622             Transhydrogenase in *Manduca sexta*. *J. Membr. Biol.* **242**, 89–94 (2011).

623     42.     Hu, X., Zhang, J. W., Persson, A. & Rydström, J. Characterization of the

624             interaction of NADH with proton pumping E. coli transhydrogenase

625             reconstituted in the absence and in the presence of bacteriorhodopsin. *BBA -*

626             *Bioenerg.* **1229**, 64–72 (1995).

627     43.     Tong, R. C. W., Glavas, N. A. & Bragg, P. D. Topological analysis of the

628             pyridine nucleotide transhydrogenase of *Escherichia coli* using proteolytic

629             enzymes. *Biochim. Biophys. Acta* **1080**, 19–28 (1991).

630     44.     Landau, M. *et al.* ConSurf 2005: the projection of evolutionary conservation

631             scores of residues on protein structures. *Nucleic Acids Res.* **33**, W299–W302

632             (2005).

633     45.     Morozenko, A., Leontyev, I. V & Stuchebrukhov, A. A. Dipole Moment and

634             Binding Energy of Water in Proteins from Crystallographic Analysis. *J. Chem.*

635             *Theory Comput.* **10**, 4618–4623 (2014).

636     46.     Pravda, L. *et al.* MOLEonline: a web-based tool for analyzing channels,

637             tunnels and pores (2018 update). *Nucleic Acids Res.* **46**, W368–W373 (2018).

638     47.     Krissinel, E. & Henrick, K. Inference of macromolecular assemblies from

639             crystalline state. *J. Mol. Biol.* **372**, 774–97 (2007).

640     48.     Krissinel, E. Crystal contacts as nature's docking solutions. *J. Comput. Chem.*

641             **31**, 133–143 (2010).

642     49.     Barad, B. A. *et al.* EMRinger: side chain–directed model and map validation

643             for 3D cryo-electron microscopy. *Nat. Methods* **12**, 943–946 (2015).

644 50. Chen, V. B. *et al.* MolProbity: all-atom structure validation for macromolecular

645 crystallography. *Acta Crystallogr. D. Biol. Crystallogr.* **66**, 12–21 (2010).

646 51. Goujon, M. *et al.* A new bioinformatics analysis tools framework at EMBL-

647 EBI. *Nucleic Acids Res.* **38**, W695–W699 (2010).

648 52. Larkin, M. A. *et al.* Clustal W and Clustal X version 2.0. *Bioinformatics* **23**,

649 2947–2948 (2007).

650 53. Pettersen, E. F. *et al.* UCSF Chimera-A visualization system for exploratory

651 research and analysis. *J. Comput. Chem.* **25**, 1605–1612 (2004).

652 54. Wu, L. N. Y., Alberta, J. A. & Fisher, R. R. [33] Purification and reconstitution

653 of bovine heart mitochondrial transhydrogenase. *Methods Enzymol.* **126**, 353–

654 360 (1986).

655

656

657    **Supplementary Information** is linked to the online version of the paper at

658    www.nature.com/nature.

659

668

669    **Author Contributions**

670    DK purified transhydrogenase, prepared cryo-EM grids, acquired and processed EM

671    data, built and analysed the atomic models and wrote the initial draft of the

672    manuscript. LAS designed and supervised the project, acquired funding, analysed data

673    and revised the manuscript.

674

675    **Author Information**

676    Affiliations: DK & LAS: IST Austria, Am Campus 1, 3400 Klosterneuburg, Austria

677    Corresponding author: LAS, sazanov@ist.ac.at

678    The authors declare no competing financial interests.

679

680    **Data availability statement**

681    Structures of "double face-down" and "single face-down" NADP$^+$ states and apo-

682    NNT were deposited in PDB with PDB access numbers 6QTI, 6QUE and 6S59,

683    respectively, with corresponding cryo-EM density maps in EMDB (EMD-4635,

684    EMD-4637 and EMD-10099).

685

686

**Extended Data Legends**

688         **Extended Data Fig. 1. Comparison of model transhydrogenases from**
689         **different species (*T. thermophilus, R. rubrum, E. coli, O. aries and H.***
690         ***sapiens*)**

691     **a**, The domain split and organisation of transhydrogenase in the four model species.
692     dII-dIII linker is conserved in all transhydrogenases, while the dI-dII linker and TM1
693     are limited to NNTs with α-β polypeptide split (e.g. *E. coli*) and single polypeptide
694     NNTs (metazoans, including mammals). TM5 is only present in metazoans. **b**,
695     Residue conservation scores (calculated in Consurf, coloured cyan to magenta from
696     low to high conservation) mapped on the structure of a single monomer of
697     transhydrogenase. The most highly conserved regions are the proton translocation
698     pathway, nucleotide binding sites and dI-dIII, dII-dIII and dI-dI interfaces. **c**, The
699     architecture of mammalian dII. Supernumerary helices TM1 and TM5 are coloured in
700     a darker shade of blue. Residues of the proton transfer pathway are shown in circles.
701     $3_{10}$-helix stretch within TM3 is depicted as a triangular helix. **d**, Alignment of
702     conserved residues on TM3, TM9, TM13, TM14 and CL7 and CL8 important for
703     proton translocation and reaction coupling in *T. thermophilus* (Tt), *R. rubrum* (Rr), *E.*
704     *coli* (Ec), *O. aries* (Oa) and *H. sapiens* (Hs). *T. thermophilus* and a handful of other
705     species with an NGXGG motif on TM9 have the protonatable histidine on TM3
706     ($α_2$H42 in *T. thermophilus*) while most other species that share an HSXXG motif on
707     TM9 have the protonatable histidine on TM9 (βH91 in *E. coli* and H664 in *O. aries*).

708

709         **Extended Data Fig. 2. Purification and biochemical characterisation of**
710         **ovine transhydrogenase**

711     **a**, Ovine NNT was purified chromatographically. The last step of purification, size
712     exclusion chromatography, in two different detergents, FOM and LMNG, is shown.
713     SDS-PAGE shows the presence of ~110 kDa polypeptide of NNT. Highest purity
714     fractions around ~10.5 mL were pooled and concentrated for cryo-EM sample
715     preparation. **c**, NNT is highly active and stable when purified in LMNG as shown by

716 undiminished activity over several days when stored at 4°C. Error bars represent
717 standard deviations based on n=3 independent measurements. **d**, Reconstitution of
718 purified NNT into DOPC liposomes shows that the reverse transhydrogenation
719 reaction is tightly coupled to proton transfer as it is stimulated ~10-fold by proton
720 gradient uncoupler CCCP and by solubilisation in CHAPS detergent. Error bars
721 represent standard deviations based on n=3 independent measurements. **e,**
722 Trypsinolysis of NNT at different pH in the presence of substrates. 110 kDa full NNT
723 and previously identified[15] 66 and 43 kDa fragments are labelled with asterisks. As
724 pH decreases from 8 to 6, NADPH-induced proteolysis diminishes relative to that
725 induced by $NADP^+$. At pH 5 trypsin produces different fragments, but stabilisation of
726 the intact NNT by NADPH is evident. Trypsinolysis was performed independently
727 three times with similar results. NNT purification was repeated independently ten
728 times with similar results as shown in panels a-b. For gel source data, see
729 Supplementary Figure 1.

730

731 **Extended Data Fig. 3. Processing of NNT-$NADP^+$ dataset**

732 Thorough classification of particles resulted in six distinct classes with different
733 domain orientations and resolutions. Best-resolution class ("double face-down" NNT)
734 is almost symmetric with both dIIIs bound in the 'face-down' position while the other
735 five have only one dIII bound in the face-down position and the other dIII detached
736 and the $dI_2$ tilted at different angles. Simultaneous opening of $dI_2$ and dissociation of
737 dIIIb is probably necessary to permit full dIIIb rotation during the catalytic cycle.
738 Monomers with dIII detached from dII also show weak or no density for dI-dII linker
739 which suggests that it detaches from dIII to allow $dI_2$ to open.

740

741 **Extended Data Fig. 4. Processing of Apo-NNT and NNT-NADPH datasets**

742 **a,** NNT bound to NADPH exhibited a large degree of conformational flexibility,
743 which prevented a high-resolution (beyond 8 Å) refinement of any class of particles.
744 Classification into 20 classes revealed that only a small proportion (~5%) of particles

745   have one dIII bound to dII in the face-down orientation (class C). Another ~10% have

746   partially detached dIII (classes A and B). A vast majority, however, have both dIIIs

747   dissociated from the other domains leading to a large degree of freedom of movement

748   of $dI_2$ and both dIIIs independently of each other (see classes D, E and F). **b,** Apo-

749   NNT exhibited a single conformational class similar to the "double face-down" NNT

750   class in the presence of $NADP^+$.

751

752   **Extended Data Fig. 5. Examples of protein and ligand cryo-EM density**

753   All examples are from the "double face-down" class in the presence of $NADP^+$,

754   unless otherwise stated. **a,** Density of the transmembrane helices lining the proton

755   channel (TM3 and 13). **b,** Density comparison of the TM2 between the "double face-

756   down" and "single face-down" (dIII-detached monomer) $NADP^+$ classes, as well as

757   apo class, which remains in the same conformation upon dII opening while TM9

758   changes (Extended Data Fig. 6c). **c,** Beta sheet density of dI. **d,** Beta sheet density of

759   dIII. **e,** $\alpha$-helical segment of dI. **f,** $\alpha$-helical segment of dIII. **g,** Two phosphatidyl-

760   cholines bound in the cavity enclosed by TM1, 2 and 6. **h,** $dIIIa-NADP^+$ density. **i,**

761   $dIIIb-NADP^+$ density. **j,** Partial $NAD^+$ density in dIa. **k,** Partial $NAD^+$ density in dIb.

762   The density for lipids and putative $NAD^+$ is discussed in Methods.

763

764   **Extended Data Fig. 6. Comparison of "double face-down" and "single**

765   **face-down" $NNT-NADP^+$ conformations and apo-NNT.**

766   **a,** Local resolution and FSC curves for the "double face-down" $NNT-NADP^+$

767   structure. **b,** Local resolution and FSC curves for the "single face-down" NNT-

768   $NADP^+$ structure. **c,** Local resolution and FSC curves for the apo NNT structure. **d,**

769   Overall comparison of "double face-down" (cyan) and "single face-down" (green)

770   classes of NNT. An increased dI tilt, dIIIb detachment and dIIb conformation change

771   are visible. **e,** Comparison of the two monomers in the "closed" $NADP^+$ class as

772   viewed from the dimerization interface reveals a tilt of $dI_2$ and asymmetry in dI-

773   dIIIa/b contacts. **f,** Overall comparison of "double face-down" $NNT-NADP^+$ (cyan)

774 and apo NNT. dII-dIII are in the same conformation and $dI_2$ is slightly more tilted in

775 the apo-NNT. **g,** Electrostatic surface potential of the proton entry cavities on the

776 matrix (bottom) and IMS sides (top) as well as that of the membrane-facing side

777 (right). **h,** Hydrophobicity of residues on the surface of $dII_2$ (coloured white to red

778 from hydrophobic to hydrophilic). Surface-exposed tyrosine and tryptophan residues,

779 which often delineate lipid membrane surface, are highlighted in green and the lipid-

780 binding pocket is circled.

781

782 **Extended Data Fig. 7. Changes in the proton translocation channel upon**

783 **dIII detachment and comparison between ovine and *T. thermophilus* dII**

784 **a**, Comparison of *T. thermophilus* dII (salmon, PDB 5UNI) and "double face-down"

785 (dIII attached) ovine dII (cyan, supernumerary TM1 and TM5 in blue). Residues in

786 the N-side cavity display markedly different conformations. **b**, Comparison of *T.*

787 *thermophilus* dII (salmon, PDB 5UNI) and "single face-down" (dIII-detached

788 monomer) ovine dII (blue). Residues in the N-side cavity match more closely as both

789 of these dII structures are detached from dIII. **c**, Comparison of the TM9 density in

790 the "double face-down", "single face-down" (dIII-detached monomer) and apo dII

791 clearly displaying a H664 flip in the dIII-detached dII. **d**, Comparison of Dowser-

792 predicted waters in the dIII-attached (cyan) and dIII-detached (green) dII. The dIII-

793 attached structure has two water molecules, one below and one above the N-side

794 proton gate while the dIII-detached structure only has one water molecule above the

795 gate, consistent with the proposal that channel is open to P-side when dIII is attached.

796 **e**, Density for a water molecule coordinated between H664 and S492, consistent with

797 Dowser-predicted water is beginning to show in our cryo-EM density. **f**, Proton

798 pathway profile (calculated in Mole 2.5) in dIII-attached dII reveals a diameter

799 constriction between N-side and H664, a hydrophobic stretch between H664 and

800 E806 and a negatively charged P-side proton entry site. **g**, Proton pathway profile in

801 the dIII-detached dII. Additional constriction appearing between H664 and P-side

802 upon dIII detachment is indicated.

803

804           **Extended Data Fig. 8. Different conformations of dIII**

805    **a,** A homology model of the asymmetric ovine NNT based on the *T. thermophilus*
806    dI$_2$dIII heterotrimer structure (PDB 4J16). N.B. putative interacting residues at the
807    dIIIup-dIIIdown interface. dI-dII linker contacts the loop D of dIII in the face-down
808    conformation. D942 and Y941 from dIII form hydrogen bonds with R544 on CL2
809    loop stabilising the dII-dIII interface. Helix 4 and loop D also contribute towards
810    formation of the dI-dIII interface but Y941 is too far to interact with dI. **b,**
811    Comparison of ovine dIII (red) with *R. rubrum* isolated dIII (PDB 1PNO: chain A in
812    blue and chain B in green). Helix 4, loop D and loop E are all more open around the
813    nucleotide in the ovine structure but the nucleotide is occluded by the interactions
814    from the dII residues (not shown) in the ovine "face-down" structure. **c**, Comparison
815    of the NADP(H) binding site in "double face-down"-NNT (left) and apo-NNT (right).
816    Loop E, K999 and R1000 are disordered in apo-NNT and R925 flips into an outward-
817    facing orientation, opening the site to the solvent.

818

819           **Extended Data Fig. 9. Validation of the mechanism and the reverse**
820           **transhydrogenation mechanism**

821    **a**, Summary of the biochemical evidence and mutagenesis data supporting the
822    proposed mechanism. Full description of mutants in *E. coli*, *R. rubrum* and human
823    patient mutations are in Supplementary Tables 1-3. **b**, Our proposal for reverse
824    reaction. Reverse transhydrogenation reaction consumes NADPH and NAD$^+$ and
825    results in proton pumping, supporting proton motive force (pmf). The driving forces
826    for this reaction are the nucleotide ratios and low pmf which promotes protonation of
827    H664 from the matrix side.

828

829           **Extended Data Table 1. Cryo-EM data collection, refinement and**
830    **validation statistics**

831

**a**

dI

NAD(H)

dIII

NADP(H)

matrix

dII

H⁺

IMS

"double face-down"

**b**

"single face-down"

"double detached"

asymmetric *(T. thermophilus)*

"double face-up" *(prohibited)*

**c**

~100 Å

~130 Å

90°

**d**

NAD⁺

NADP⁺

90°

Fig. 1

**a**

Apo: "double face-down"

NADP⁺: "double face-down"

NADP⁺: "single face-down"

100 %
4.2/3.7 Å

63 %
3.2/2.9 Å

18 %
4.1/3.7 Å

NADPH: "single face-down"

NADPH: "double detached"

NADPH: "double detached"

dIIIa attached to dII

dIIIa detached

weak dIIIb density

dIIIa detached

dI-dII linkers

11 %
8.6 Å

11 %
9.2 Å

11 %
11.1 Å

**b**

90°

90°

Fig. 2

Fig. 3

a

dIII-attached
dIII-detached

CL8    TM14

TM9    TM13

TM3

N489

H664    N796

S799

CL6    CL7

90°

11    12    10    9

13

*

14    3

CL8

90°

N489

H664    S799    N796

b

loop E

dI-II linker
dIII contact

loop D

helix 4

CL8

c

TM13

R925    M926

Y890

TM9

Fig. 4

hydride transfer

dIII flip and opening, proton channel opening to P-side

**1**
dI · dII · dIII · NADH * · NADP⁺ · H664

**2**
dI · dII · dIII · NADPH · H664 · H⁺

forward reaction

dIII detachment and closing, proton channel opening to N-side

**4**
dI · dII · dIII · NADP⁺ · H⁺ · H664

**3**
dI · dII · dIII · NADPH · NADP⁺ · H664⁺

nucleotide exchange

Fig. 5

ED 1

ED 2

2272 movies collected

MotionCor2 and CTFFind

2160 good images selected
Autopicking
1076677 particles extracted
2D Classification
840663 particles retained after 2D classification

3D Classification
T=4, pixel size = 3.21 Å

395240 particles, pixel size = 2.13 Å

3D Classification, T=12

342284 particles, pixel size = 1.065 Å

dII2dIII2 mask
3.5 Å

3D Classification without searches, T=10

98294 particles

58441 particles

23820 particles

21577 particles

68179 particles

71973 particles

CTF refinement and polishing

CTF refinement and polishing

"double face-down" NNT
3.2 Å full
2.9 Å dII2dIII2
3.2 Å dI2

"single face-down" NNT
4.0 Å full
3.5 Å dII2dIII
4.1 Å dI2

7 Å

7 Å

13 Å

13 Å

Further classification around dIIIb
Refinement of particles without any recognisable dIIIb density

3.7 Å dII2dIII
28498 particles

ED 3

**a**

1724 movies collected

MotionCor2 and CTFFind

3D Classification

1603 good images selected
Autopicking
516395 particles extracted
2D Classification
510073 particles retained after 2D classification

T=4, pixel size = 3.21 Å

405141 particles, pixel size = 3.21 Å

2nd 3D classification with k=20, T=8

A 5.6%, 11.1 Å
B 5.3%, 9.2 Å
C 5.4%, 8.6 Å
D 5.9%, 16 Å
E 6.5%, 16 Å
F 5.4%, 16 Å

**b**

786 movies collected

MotionCor2 and CTFFind

643 good images selected
Autopicking
500001 particles extracted
3D Classification

T=6, pixel size = 2.52 Å

4.5 Å

AutoRefine
283706 particles, pixel size = 0.84 Å

Focus-refinement on dIIdIII

4.3 Å

Further classification around dIIdIII to improve resolution
3D Classification without searches, T=12, dIIdIII mask

Bayesian polishing

67908 particles

same particle selection

Bayesian polishing

3.9 Å

Bayesian polishing

3.7 Å

4.2 Å

ED 4

**a**

TM3    TM13

**b**

TM2: NADP+ "double face-down"

TM2: NADP+ "single face-down"

TM2: apo "double face-down"

**c**    90°

**d**    90°

**e**

**f**

**g**

**h**    **i**    **j**    **k**

ED 5

**a** "double face-down" NNT-NADP^{+}

**b** "single face-down" NNT-NADP^{+}

**c** "double face-down" apo-NNT

**d** NNT-NADP^{+}: "Double face-down" vs. "single face-down"

**e** chain A          chain B

**f** "Double face-down": NADP^{+} vs. apo

**g** IMS          side-view          matrix          −5 charge +5

**h** matrix          IMS

ED 6

**a** **dIII-attached** vs. *T. thermophilus* dII (5uni)

**b** **dIII-detached** vs. *T. thermophilus* dII (5uni)

N-side

P-side

90°    90°

TM3
S492 H42
N489 N39
N211
N796
T214
N89 S799
TM9 H664 TM13

TM3
N39 S492
N489 H42
N211
N796
S799
N89 T214
TM9 H664 TM13

**c**

H664    H664    H664

TM9
NNT-NADP⁺
dIII-attached

TM9
NNT-NADP⁺
dIII-detached

TM9
apo-NNT
dIII-attached

**d** **dIII-detached** vs. **dIII-attached**

N489
N796
H664 S799

**e** **dIII-attached**

H664
N796 N489
S799 S492

**f** **dIII-attached**

matrix    membrane    IMS

Distance    Charge
2 Å    Radius
0 Å    46.7 Å
2 Å    Radius
Distance    Hydropathy

diameter    H664    hydrophobic    E806
constriction    N796    patch
N489

**g** **dIII-detached**

Distance    Charge
2 Å    Radius
0 Å    41.3 Å
2 Å    Radius
Distance    Hydropathy

diameter    H664    diameter    hydrophobic    E806
constriction    N796    constriction    patch
N489

ED 7

ED 8

**a**

**NAD(H)-binding site**
*Y245, R139*
full inhibition

**dI-dI interface**
*Y158, F172*
dI cannot dimerise, full inhibition of activities

**NADP(H)-binding site**
*H920, A923, E967, K999*
decoupled or fully inhibited phenotype

**trypsinolysis of dI-dII linker and CL4** stimulated by NADPH at high pH and NADP+ at low pH

**loop E**
*Y1006, G1005*
decoupled phenotype in full NNT increased reaction rate in dI-dIII system

**NADP⁺-dependent cyclic reaction**
low pH optimum

**C893 labelling**
stimulated by NADPH at high pH

**dII-dIII interface**
*R544, D787, R839*
decoupled phenotype or stimulated cyclic activity (locked in dIII-detached state)

**proton translocation pathway**
*H664, N796*
*(small and/or neutral mutants)*
locked in dIII-attached state

**proton translocation pathway**
*H664, T709, N796, G826*
*(bulky and/or charged mutants)*
locked in dIII-detached state

**proton translocation pathway**
*S799*
decoupled phenotype

**b**

hydride transfer

dIII flip and opening, proton channel opening to P-side

reverse reaction

nucleotide exchange

dIII detachment and closing, proton channel opening to N-side

ED 9

| | NNT-NADP+ "double face-down" (EMD-4635) (PDB 6QTI) | NNT-NADP+ "single face-down" (EMD-4637) (PDB 6QUE) | Apo-NNT "double face-down" (EMDB-10099) (PDB 6S59) |
|---|---|---|---|
| **Data collection and processing** | | | |
| Magnification | 130000x | 130000x | 130000x |
| Voltage (kV) | 300 | 300 | 300 |
| Electron exposure (e–/Å²) | 72 | 72 | 90 |
| Defocus range (µm) | ~ -1 to -2.5 | ~ -1 to -2.5 | ~ -1 to -2.5 |
| Pixel size (Å) | 1.065 | 1.065 | 0.84 |
| Symmetry imposed | C1 | C1 | C1 |
| Initial particle images (no.) | 1076677 | 1076677 | 500001 |
| Final particle images (no.) | 98294 | 58441 | 67908 |
| Map resolution (Å) | $dI_2$ – 3.2 Å, $dII_2dIII_2$ – 2.9 Å | $dI_2$ – 4.2 Å, $dII_2dIII$ – 3.7 Å | $dI_2$ – 4.5 Å, $dII_2dIII_2$ – 3.7 Å |
| FSC threshold | 0.143 | 0.143 | 0.143 |
| | | | |
| **Refinement** | | | |
| Initial model used (PDB code) | dI and dII built de novo, dIII based on 1D4O | 6QTI | 6QTI |
| Model resolution (Å) | $dI_2$ – 3.4 Å, $dII_2dIII_2$ – 3.1 Å | $dI_2$ – 4.3 Å, $dII_2dIII$ – 4.0 Å | $dII_2dIII_2$ – 3.8 Å |
| FSC threshold | 0.5 | 0.5 | 0.5 |
| Map sharpening $B$ factor (Å²) | $dII_2dIII_2$ -36.2 | $dII_2dIII$ -55 | $dII_2dIII_2$ -67.3 |
| | $dI_2$ -50.2 | $dI_2$ -77.0 | $dI_2$ -197.5 |
| Model composition | | | |
| Non-hydrogen atoms | 15996 | 13791 | 13397 |
| Protein residues | 2076 | 1865 | 2066 |
| Ligands | 14 | 3 | 8 |
| $B$ factors (Å²) | | | |
| Protein | 74.0 | 128.0 | 115.8 |
| Ligand | 114.8 | 172.8 | 143.5 |
| R.m.s. deviations | | | |
| Bond lengths (Å) | 0.0071 | 0.008 | 0.0085 |
| Bond angles (°) | 1.29 | 1.30 | 1.36 |
| Validation | | | |
| MolProbity score | 1.56 | 1.66 | 1.59 |
| EMRinger score | 3.58 | 1.73 | 2.53 |
| Clashscore | 3.37 | 4.26 | 3.50 |
| Poor rotamers (%) | 0 | 0.21 | 0.44 |
| Ramachandran plot | | | |
| Favored (%) | 93.44 | 92.85 | 92.95 |
| Allowed (%) | 6.56 | 7.05 | 7.05 |
| Disallowed (%) | 0 | 0.1 | 0 |

ED 10

**Supplementary Information**

**Supplementary Discussion**

<u>Mammalian-specific features of NNT</u>

The twelve conserved transmembrane helices in mammalian NNT adopt the same fold as demonstrated in the isolated *T. thermophilus* dII domain[1,2]. The supernumerary helices TM1 and TM5 form an unexpected extended dII dimer interface. Relatively large tilt of the TM1 allows its strong association over a large contact area with the TM5 of the opposite monomer, possibly stabilizing dimer formation in mammals (Fig. 3a). The connection from the dI domain via TM1 to TM5 of the opposing monomer may also help in the coordination of the catalytic cycle events between the monomers as discussed below.

The dI-dII linker present in transhydrogenases with single and double polypeptide split (Extended Data Fig. 1a) was resolved here for the first time. The C-terminal part of the linker (residues 410-424) forms a loosely defined α helix which contacts dIII in the 'face-down' orientation. V412 and T411 from the linker interact with residues N974-P977 of the loop D (residues 974-986) on dIII. This explains why K410-T411 bond is protected from trypsinolysis in the apo and NADP$^+$-bound state (Fig. 1c,d, Extended Data Fig. 8a)[3]. The N-terminal region of the dI-dII linker (400-410) is a flexible loop and only displays very weak density. In the dIII-detached state, the density for the C-terminal part of the linker disappears, which could indicate partial unfolding of the helix to accommodate an increased distance between dI and dII.

The only catalytically important conformation that we did not observe in our structures is the face-up dIII conformation since it is likely that the dI-dIII interface formation requires binding of the corresponding nucleotide to dI and, once formed, has a very short life span as the hydride transfer is fast[4–6]. In contrast to the bacterial enzymes, the architecture of mammalian NNT with its dI-dII linker may prevent the observation of a stable face-up dIII conformation, although this remains to be established in future studies. Structures of dI$_2$dIII heterotrimers from *T. thermophilus* and *R. rubrum* demonstrated that only one copy of dIII can bind to dI$_2$ at a time due to steric clashes[7–10]. The symmetry of the "double face-down" state, most likely specific to single polypeptide transhydrogenases, is broken due to the tilting of dI$_2$, which interacts loosely with dIII in one monomer (dIIIa) and not at all in another (dIIIb) (Extended Data Fig. 6e). The overall architecture of the dimer does not allow for tight

interactions between dI and dIII in both monomers, whether dIII is facing "up" or "down". On the other hand, dIII-dII interaction is permitted in both monomers simultaneously.

Comparison of proton translocation machinery between ovine and *T. thermophilus* NNT

All transhydrogenases have a single key protonatable histidine at the N-side of dII, either on TM3 ($\alpha_2$H42 in *T. thermophilus*) or on TM9 in *E. coli* and mammals ($\beta$H91/H664) (Extended Data Fig. 1d and 7a,b). MD simulations of *T. thermophilus* enzyme[2] showed that protonation of this histidine induces a transient opening of the transmembrane proton channel between $\alpha_2$H42 and $\beta$E221 (ovine H664 and E806) accompanied by a flip of $\beta$T214. This role could be played by the ovine homologue S799 or by S492, a homologue of *T. thermophilus* $\alpha_2$H42, or by a non-conserved T495 (Fig. 3b)[2]. The latter two residues sit on a clear and significant distortion of helix TM3, i.e. two turns of $3_{10}$ helix (the only such distortion in dII, Fig. 3b). A similar distortion is present (but was not discussed) around $\alpha_2$H42 in the TM3 of *T. thermophilus* dII (PDB 5UNI and 4O93). Furthemore, in TM9, the backbone oxygen atoms of residues 661, 662 and 667 are facing away from the helix-forming hydrogen bond network. Such disruptions of secondary structure in TM helices happen almost exclusively in functionally important sites, where flexibility of otherwise rigid TM helices is required[11,12], consistent with our conclusion that these key TM3 and TM9 residues undergo conformational changes associated with proton translocation during the catalytic cycle, as observed in dII upon dIII attachment/detachment (Fig. 4).

The differences between ovine and *T. thermophilus* dII are also in the P-side (intermembrane space) cavity, gated by a conserved residue E806 which in ovine dII is in an extended conformation in contrast to the *T. thermophilus* structures, with T674 and E678 allowing access to the P-side. Residues at the P-side of the proton transfer path are generally much less conserved between species than at the N-side. The P-side entry cavity in mammals also has a stronger negative charge (Extended Data Fig. 6g), appropriate for the attraction of protons in the forward reaction.

In contrast to what has been suggested for the *T. thermophilus* enzyme, dIII attachment to dII does not change the conformation of the short lateral helix CL8 nor does it disrupt the conserved salt bridge R839-D787 (Extended data Fig. 8c)[1].

Detailed explanation of the mechanism

As outlined in the main text, the excess of NADP$^+$ and pmf will promote forward reaction in the cycle shown in Fig. 5. After a full cycle and hydride transfer back at step 1, subsequent dIII dissociation from dI in step 2 is unlikely to be initiated by hydride transfer itself as it is a fast step and dI$_2$dIII structures were solved with many combinations of bound nucleotides[7,10]. However, NNT always operates as a dimer, in which the two dIII domains cannot simultaneously attach to the dI dimer, as noted above. Therefore, as the second monomer (in grey in Fig. 5) goes through a similar cycle as the first monomer (in colour), the second dIII, swivelling up after detachment from dII, will clash with the already bound dIII from the first monomer and dislodge it, initiating its flip "down" in step 2, resuming the cycle. This sequence of events ensures tight coupling between hydride transfer, nucleotide exchange and proton translocation. "Slipping", or uncoupling, at any step is prevented because proton translocation cannot happen without nucleotide exchange. For example, step 3 (Fig. 5) cannot progress to step 4 and switch proton channel access unless there is nucleotide exchange – only the dIII-NADP$^+$ and H664$^+$ combination will allow dIII dissociation and dII opening to the N-side. If nucleotide exchange does not happen, bound dIII-NADPH will interact strongly with H664$^+$ and prevent dIII detachment and dII opening to the N-side. In other words, two half-paths of proton across the membrane (up to H664 and after) in both forward and reverse reactions are connected only by nucleotide exchange, excluding any uncoupling.

In the reverse reaction, when pmf is low and there is an excess of NADPH, all the steps are naturally reversed, resulting in proton pumping into the P-side (Extended Data Fig. 9b). After hydride transfer, dIII-NADP$^+$ is dislodged by an incoming dIII from the opposing monomer and is attached to dII with protonated H664$^+$ (as pH is now lower in the matrix) (steps 1-2). This opens the channel to the P-side and H664 loses its proton there, as its pK$_a$ is reduced due to interaction with NADP$^+$ (step 2). Nucleotide exchange follows due to the excess of NADPH (step 3) and dIII-NADPH swivels "up", due to its low affinity to neutral H664, back to step 1. In both forward and reverse reactions, NAD$^+$/NADH formed in dI in step 1 would be exchanged for NADH/NAD$^+$ before step 4 completes, so that the cycle can resume, since dI remains open throughout.

The proposed mechanism ensures tight coupling also close to the equilibrium conditions. We can simply consider all possibilities. After hydride transfer in step 1, dIII associates with dII, allowing nucleotide exchange. Subsequent to nucleotide exchange possible scenarios will be as follows:

1.      If it is dIII-NADP+ and H664$^+$ (weak dIII-dII interaction), then dIII would be flipped up first, then dII is closed from periplasm and opened to cytoplasm, so that proton is released into the cytoplasm – this is forward reaction, when there is excess of NADP$^+$.

2.      If it is dIII-NADP$^+$ and H664 (strong dIII-dII interaction), dIII will remain attached to dII until H664 is protonated from the periplasm. This prevents slipping of forward reaction. After H664 protonation dIII will be flipped up and proton released into the cytoplasm, in the forward reaction as above.

3.      If it is dIII-NADPH and H664 (weak dIII-dII interaction), dIII will flip up first, then dII will close to the periplasm and open to cytoplasm, allowing H664 protonation from the cytoplasm - this is reverse reaction, when there is excess of NADPH.

4.      If it is dIII-NADPH and H664$^+$ (strong dIII-dII interaction), dIII will remain attached to dII until H664 is de-protonated into the periplasm. This prevents slipping of reverse reaction. After H664 de-protonation, dIII can flip up and dII will close to the periplasm and open to cytoplasm, allowing H664 protonation from the cytoplasm, in the reverse reaction as above.

5.      In the apo state, dIII remains attached to dII, preventing proton leak.


Thus, we achieve tight coupling between hydride transfer and proton translocation, without any slipping, at all conditions – either favourable for forward or reverse reaction, or close to equilibrium. Close to equilibrium the overall net direction of reaction will depend on the pmf value and nucleotide ratios.


Communication between the two monomers

The mechanism outlined above and previous biochemical data imply strong coupling between the two monomers resulting in their 'anti-phase' action. Our structures suggest different ways in which the two monomers can communicate with each other, in addition to one dIII dislodging another one from dI.

Rotation of one dIII into the face-up position (modelled on dI$_2$dIII crystal structures) would bring the two dIII domains much closer together than in the "double face-down" structure, so that they can form many hydrogen bonds without clashing and so interact when swivelling (Extended Data Fig. 8a).

dI dimer is stabilised by a large buried surface extended by an elongated hairpin (ovine residues 172-184) reaching out from each monomer into the neighbour[8,13,14]. The hairpin from one dI monomer interacts only weakly or not at all with the "face-down" dIII in

another monomer (as seen in our structures), but strongly with the "face-up" dIII (as in dI$_2$dIII crystal structures). This hairpin originates directly from the Rossmann fold coordinating the NAD(H) in the first monomer, which may allow for communication of the redox state from one dI monomer to the other.

Additionally, in mammalian enzyme the dI-dII linker contacts the dIII from one monomer and is continued by the TM1, which forms extensive interactions with the TM5 and the TM4-5 loop from another monomer, which in turn directly contact dIII from that monomer (Fig. 1d). This feature, in addition to the TM1/TM5 dimer stabilisation, may allow for more efficient dIII cross-talk. Together, all these possible routes of communication may allow for the two monomers to work more effectively in an anti-phase fashion.

## Supplementary Table 1. Catalytic activities of site-directed mutants in *E. coli* NNT

| Homol-ogous ovine residue | *E. coli* mutation | Reverse activity | Cyclic activity | Proton pumping activity | Notes | Structural and mechanistic explanation if conserved | Reference |
|---|---|---|---|---|---|---|---|
| D214 | D195E | 8% | N/A | N/A | forward activity inhibited by ~79% | part of the NAD(H)-binding pocket | [15] |
| Y245 | Y226F | ~40% | N/A | 31% | ~3x increase in $K_m$ for APAD$^+$ | part of the NAD(H)-binding pocket - mobile loop | [16] |
| Y245 | Y226L | 38% | N/A | 13% | ~3x increase for APAD$^+$ | part of the NAD(H)-binding pocket - mobile loop | [16] |
| Y245 | Y226H | 45% | N/A | 28-42% | ~3x increase for APAD$^+$ | part of the NAD(H)-binding pocket - mobile loop | [16] |
| Y245 | Y226N | 43% | N/A | 51% | N/A | part of the NAD(H)-binding pocket - mobile loop | [16] |
| K251 | D232N | 45% | N/A | 67% | N/A | | [17] |
| K251 | D232E | 89% | N/A | 110% | N/A | | [17] |
| K251 | D232K | 75% | N/A | 65% | N/A | | [17] |
| K251 | D232H | 84% | N/A | 98% | N/A | | [17] |
| E257 | E238Q | 71% | N/A | 18% | N/A | part of the NAD(H)-binding pocket | [17] |
| E257 | E238K | 41% | N/A | 27% | N/A | part of the NAD(H)-binding pocket | [17] |
| K259 | E240Q | N/A | N/A | N/A | 3x increased $K_m$ for APAD$^+$ but not for NADH | | [17] |
| | triple D232N E238Q E240Q | 55% | N/A | 59% | lower inhibition by DCCD than wt, both in the presence and absence of NAD(P)H | | [17] |
| | triple D232H E238Q E240Q | 44% | N/A | 51% | lower inhibition by DCCD than wt, both in the presence and absence of NADH(P)H | | [17] |
| A454 | E423C | >75% | N/A | N/A | | | [18] |
| Y470 | Y439F | 41% | N/A | 38% | | part of the lipid binding pocket at the dimer interface | [19] |
| A479 | A448C | 50-75% | N/A | N/A | | part of the dII-dIII interface | [18] |
| H481 | H450T | 17% | N/A | 51% | Greatly lowered activity but still pumps protons | part of the dII-dIII interface | [20] |
| H481 | H450T | 26% | 3000% | 21% | | part of the dII-dIII interface | [21] |
| T488 | T457A | 80% | N/A | 109% | | immediate vicinity to the proton pumping residue N489 | [19] |
| N489 | N458A | 66% | N/A | 44% | | part of the proton pumping machinery | [19] |
| S492 | S461 | 51% | N/A | 67% | | immediate vicinity to the proton pumping residue N489 | [19] |
| | triple T457A N458A S461A | 9% | N/A | 22% | | | [19] |
| G505 | Q474C | >75% | N/A | N/A | | | [18] |
| L507 | G476C | 93% | 81% | N/A | double mutants with cysteines on other cytoplasmic loops generated and cross-linked; activities were mainly preserved (above 50%) | | [22] |
| N527 | N492A | 54% | N/A | 78% | | immediate vicinity to the proton pumping residue N489 | [19] |
| L533 | T498C | >75% | N/A | N/A | | | [18] |
| T535 | T500A | 49% | N/A | 56% | | not part of proton transfer pathway | [19] |
| Q536 | Q501C | >75% | N/A | N/A | | not part of proton transfer pathway | [18] |
| R537 | R502S | 71% | N/A | 93% | | not part of proton transfer pathway | [17] |
| 540-545 | Δ(505-510) | 6% | 371% | N/A | NADP$^+$ independent cyclic activity increased by 35x - enzyme co-purifies with NADP$^+$ at 0.2 mol/mol | CL2 (esp. R544) is important for dII-dIII interface formation, deletion of this loop locks the enzyme in the dIII-detached state, explaining the copurification with NADP+, increased cyclic activity and decreased | [23] |

| | | | | | | | |
|---|---|---|---|---|---|---|---|
| | | | | | | reverse activity, because NADP(H) cannot exchange without dIII interacting with dII | |
| 543-545 | Δ(508-510) | 50% | 253% | N/A | NADP$^+$ independent cyclic activity increased by 306% | CL2 (esp. R544) is important for dII-dIII interface formation, deletion of this loop locks the enzyme in the dIII-detached state, explaining the increased cyclic activity and decreased reverse activity, because NADP(H) cannot exchange without dIII interacting with dII | [23] |
| R544 | K509E | 50% | 201% | N/A | NADP$^+$ independent cyclic activity increased by 168% | R544 important for dII-dIII interface formation, mutation of this residue locks the enzyme in the dIII-detached state, explaining the increased cyclic activity and decreased reverse activity, because NADP(H) cannot exchange without dIII interacting with dII | [23] |
| G573 | S2C | 100% | 95% | N/A | | | [18,22] |
| L595 | L24C | ~15% | N/A | N/A | | not part of proton transfer pathway, buried residue | [18] |
| A601 | S30C | >75% | N/A | N/A | | | [18] |
| R602 | R31A | 19% | 8% | 8% | | stabilises CL3, TM5 and TM6 | [24] |
| R602 | R31E | >120% | 61% | >120% | | stabilises CL3, TM5 and TM6 | [24] |
| R602 | R31L | 41% | 15% | 46% | | stabilises CL3, TM5 and TM6 | [24] |
| N605 | N34A | 59% | N/A | 79% | | not part of proton transfer pathway | [19] |
| N605 | N34T | >120% | 92% | >120% | | not part of proton transfer pathway | [24] |
| P627 | T54C | 50% or >75% | 65% | N/A | | | [18,22] |
| K649 | K76Q | 99% | 95% | ~100% | | not part of proton transfer pathway | [24] |
| R650 | K77A | 9% | 4% | 11% | | | [24] |
| R650 | K77L | 13% | 4% | 19% | | | [24] |
| R650 | K77Q | 49% | 46% | 62% | | | [24] |
| S654 | T81C | 50-75% | N/A | N/A | | | [18] |
| D655 | E82K | 79% | N/A | 66% | | | [20] |
| D655 | E82Q | 63% or 49% | N/A | 85% or 63% | | | [19,20] |
| Q658 | E85A | 9% | 19% | 9% | | N-terminal part of the TM9 which undergoes changes during dIII attachment | [24] |
| Q658 | E85C | 4% or 50-75 | 3% | 8% | | N-terminal part of the TM9 which undergoes changes during dIII attachment | [18,24] |
| Q658 | E85K | 15% | 4% | 14% | | N-terminal part of the TM9 which undergoes changes during dIII attachment | [24] |
| Q658 | E85L | 8% | 5% | 7% | | N-terminal part of the TM9 which undergoes changes during dIII attachment | [24] |
| Q658 | E85Q | 3% or 63% | 2% | 4% or 71% | | N-terminal part of the TM9 which undergoes changes during dIII attachment | [19,24] |
| Q658 | E85S | 22% | 6% | 20% | | N-terminal part of the TM9 which undergoes changes during dIII attachment | [24] |
| | triple E79Q E82Q E85Q | 55% | N/A | 94% | | | [19] |
| H664 | H91A | 7% | 10% | 0% | H664 is a key residue for proton translocation and based on its protonation state stabilises face-down dIII-NADP$^+$ or dIII-NADPH | Mutation to small and nonpolar residue stabilised NNT in a face-down conformation, hence no cyclic or reverse activity measurable | [24] |
| H664 | H91C | 12% or 3% or 24% | 11% | 7% or 0% or 0% | No conformational change in β chain induced by NADP(H) binding - as measured by βR265 susceptibility to trypsin | Mutation to small and uncharged residue stabilised NNT in a face-down conformation, hence no cyclic or reverse activity measurable and NADP(H) cannot induce change of conformations | [20,24,25] |
| H664 | H91D | 9% or 25% | 240% or 12% | 6% or 0% | | Cyclic activity data conflicting; NNT could be trapped either in dIII-attached or detached conformations; based on H91E mutation, dIII-attached conformation is more likely | [24,26] |
| H664 | H91E | 15% | 3% | 0% | | Negatively charged residue stabilised NNT in a face-down conformation; hence no cyclic or reverse activity | [24] |
| H664 | H91G | 27% | 15% | 0% | | Mutation to small and uncharged residue stabilised NNT in a face-down conformation, hence radically reduced cyclic or reverse activities | [24] |
| H664 | H91I | 28% | 6% | 2% | | Mutation to nonpolar residue stabilised NNT in a face-down conformation, hence radically reduced cyclic | [24] |

| | | | | | | | |
|---|---|---|---|---|---|---|---|
| | | | | | | and reverse activities | |
| H664 | H91L | 18% | 11% | 2% | | Mutation to nonpolar residue stabilised NNT in a face-down conformation, hence radically reduced cyclic and reverse activities | [24] |
| H664 | H91K | 4% or 2% or 5% or 4% | 260% or 120% or 3-20% | 20% or 30% or 1% | Also increases NADP$^+$ independent cyclic activity by 40x - copurifies with 0.2 mol NADP$^+$ per mol; present in NADP(H) induced conformation as shown by susceptibility to trypsinolysis at βR265; Measured at large nucleotide conc. (0.5mM NADPH, 1mM APAD for reverse; 1mM NADH or 0.5mM NADP$^+$ and NADH each); | positive charge on H91 promotes dissociation of dIII- NADP$^+$, hence increased cyclic activity and co-purification with NADP$^+$; substitution for a bulky Lys at this crucial site prevents NADP(H) insertion and locks dII in the detached state | [23–27] |
| H664 | H91M | 16% | 3% | <1% | | Mutation to nonpolar residue stabilised NNT in a face-down conformation, hence radically reduced cyclic and reverse activities | [24] |
| H664 | H91N | 80% or 86% or 66% or 18% | 8% or 44% | 7% or 0% or 0% or 7% or 4% | Proton transfer activity is inhibited | NNT trapped in the face-down conformation; Asn cannot be protonated, hence complete inhibition of proton transfer and reduced reverse/cyclic activities as detachment of dIII is dysregulated | [21,24–26] |
| H664 | H91R | 1% or 7% | 228% or 8% | 25% or 0% | pH dependence of reverse activity disrupted - shifted towards acidic pH, pH dependence of cyclic activity stays the same; retains 0.8 mol NADP(H) per dimer | consistent with H91K mutant: positive charge on H91 promotes dissociation of dIII- NADP$^+$, hence increased cyclic activity and co-purification with NADP$^+$; NADP(H) cannot insert into dII stabilised in N-side open state | [26] |
| H664 | H91S | 19% or 6% | N/A | 11% or 8% | No conformational change in β chain induced by NADP(H) binding - as measured by βR265 susceptibility to trypsin | Mutation to small and uncharged residue stabilised NNT in a face-down conformation; hence no reverse activity measurable and NADP(H) cannot induce change of conformations | [20,25] |
| H664 | H91T | 11% or 2% | N/A | 8% or 8% | No conformational change in β chain induced by NADP(H) binding - as measured by βR265 susceptibility to trypsin | Mutation to small and uncharged residue stabilised NNT in a face-down conformation; hence no reverse activity measurable and NADP(H) cannot induce change of conformations | [20,25] |
| H664 | H91V | 17% | 3% | 0% | | Mutation to small and non-polar residue stabilised NNT in a face-down conformation; hence no cyclic or reverse activity measurable and NADP(H) cannot induce change of conformations | [24] |
| H664 | H91W | 3% | 3% | 0% | | Bulky residue stabilised dII in a dIII-attached state, hence no reverse and cyclic activities | [24] |
| H664 | H91Y | 7% | 8% | 1% | | Bulky residue stabilised dII a dIII-attached state, hence no reverse and cyclic activities | [24] |
| S665 | S92A | >120% or 53% | 95% | >120% or 78% | | not part of proton transfer pathway | [19,24] |
| S665 | S92C | >75% | N/A | N/A | | not part of proton transfer pathway | [18] |
| G668 | G95A | 56% | 45% | 44% | no cyclic activity without NADPH; rev. act measured at 200 µM substrates, cyclic at 10 µM NADPH | not part of proton transfer pathway | [28] |
| E678 | S105C | 37% or >75% | 85% | N/A | | | [18,22] |
| I681 E682 | double H108N H109N | 51% | N/A | 69% | | | [19] |
| E682-F685 | deltaH109-G112 | 58% | 49% | N/A | β domain was split into two my introducing a stop codon at H109 | | [29] |
| T688 | A114C | ~15% | N/A | N/A | | | [18] |
| V698 | E124C | 15% | >100% | N/A | pH dependence of reverse activity shifted toward acidic - max. rate at pH6 | | [22] |
| V698 | E124K | 46% | 30% | 36% | | | [24] |
| V698 | E124A | 28% | 68% | 41% | | | [24] |
| V698 | E124Q | 41% | N/A | 150% | | | [19] |
| G706 | G132A | 101% | 70% | 101% | no cyclic activity without NADPH; rev. act measured at 200 µM substrates, cyclic at 10 µM NADPH | not part of proton transfer pathway | [28] |
| T709 | T135A | 73% | 52% | 31% | | not part of proton transfer pathway but in close vicinity to be able to distort local environment | [24] |
| T709 | T135C | 55% | 13% | 16% | | not part of proton transfer pathway but in close vicinity to be able to distort local environment | [24] |

| | | | | | | | |
|---|---|---|---|---|---|---|---|
| T709 | T135D | 71% | 6% | 28% | | not part of proton transfer pathway but in close vicinity to be able to distort local environment | [24] |
| T709 | T135K | 5% | 100% | 1% | | not part of proton transfer pathway but in close vicinity to be able to distort local environment; bulky residue could stabilise detached dII, giving rise to retained cyclic activity | [24] |
| T709 | T135L | 33% | 77% | 9% | | not part of proton transfer pathway but in close vicinity to be able to distort local environment; bulky residue could stabilise detached dII, giving rise to retained cyclic activity | [24] |
| T709 | T135S | 23% | 17% | 12% | | not part of proton transfer pathway but in close vicinity to be able to distort local environment | [24] |
| S711 | T137A | 100-120% | 70% | 100-120% | | not part of proton transfer pathway | [24] |
| G712 | G138A | 57% | 34% | 32% | no cyclic activity without NADPH; rev. act measured at 200 μM substrates, cyclic at 10 μM NADPH | not part of proton transfer pathway | [28] |
| S713 | S139A | 6% | 12% | 0% | | not part of proton transfer pathway but in close vicinity to be able to distort local environment | [24] |
| S713 | S139C | 34% | 63% | 33% | | not part of proton transfer pathway but in close vicinity to be able to distort local environment | [24] |
| S713 | S139D | 2% | 4% | 0% | | not part of proton transfer pathway but in close vicinity to be able to distort local environment | [24] |
| S713 | S139G | 83% | 31% | 41% | | not part of proton transfer pathway but in close vicinity to be able to distort local environment | [24] |
| S713 | S139H | 1% | 2% | 0% | | not part of proton transfer pathway but in close vicinity to be able to distort local environment | [24] |
| S713 | S139K | 2% | 4% | 0% | | not part of proton transfer pathway but in close vicinity to be able to distort local environment | [24] |
| S713 | S139L | 4% | 6% | 0% | | not part of proton transfer pathway but in close vicinity to be able to distort local environment | [24] |
| S713 | S139N | 3% | 3% | 0% | | not part of proton transfer pathway but in close vicinity to be able to distort local environment | [24] |
| S713 | S139T | 96% | 77% | 71% | | not part of proton transfer pathway but in close vicinity to be able to distort local environment | [24] |
| S713 | triple T135A T137A S139A | 29% | N/A | 155% | | | [19] |
| A716 | A142C | >75% | N/A | N/A | | not part of proton transfer pathway but in close vicinity to be able to distort local environment | [18] |
| K719 | K145A | 44% | 21% | 50% | | Important for maintaining integrity of dII (stabilises CL6 by salt bridge to the main chain), hence inhibition of all activities | [24] |
| K719 | K145E | 46% | 57% | 67% | | Important for maintaining integrity of dII (stabilises CL6 by salt bridge to the main chain), hence inhibition of all activities | [24] |
| K719 | K145L | 19% | 23% | 2% | | Important for maintaining integrity of dII (stabilises CL6 by salt bridge to the main chain), hence inhibition of all activities | [24] |
| K719 | K145T | 29% | N/A | 71% | | Important for maintaining integrity of dII (stabilises CL6 by salt bridge to the main chain), hence inhibition of all activities | [19] |
| I723 | K149Q | 49% | 58% | 67% | | | [24] |
| A727 | K153A | 17% | 16% | 19% | | | [24] |
| A727 | K153Q | 50% | 60% | 7% | | | [24] |
| L731 | A157C | >75% | N/A | N/A | | | [18] |
| R734 | R160A | 45% | 18% | 3% | | Important for maintaining integrity of dII (stabilises CL6 by salt bridge to the main chain of CL8), hence inhibition of all activities | [24] |
| R734 | R160L | 97% | 40% | 68% | | Important for maintaining integrity of dII (stabilises CL6 by salt bridge to the main chain of CL8), hence inhibition of all activities | [24] |
| H735 | H161S | 90% | N/A | 100% | | not part of proton transfer pathway or structurally important | [20] |
| H735 | H161T | 88% or 98% | 122% | 108 or 110% | | not part of proton transfer pathway or structurally important | [20,21] |
| H735 | H161C | 59% | N/A | 94% | Little effect | not part of proton transfer pathway or structurally important | [20,21] |
| N738 | N164T | >120% | >120% | 100-120% | | not part of proton transfer pathway or structurally important | [24] |
| G747 | L173C | 50-75% | N/A | N/A | | | [18] |
| S757 | S183C | 50% or | 65% | N/A | | faces the IMS, no catalytic role | [18,22] |

| | | >75% | | | | | |
|---|---|---|---|---|---|---|---|
| S767 | I193C | N/A | N/A | N/A | | no catalytic role | [18] |
| A782 | S208C | >75% | N/A | N/A | | | [18] |
| D787 | D213A | 13% | 14% | 4% | | Important for integrity of dII and transmission of conformational changes between dII and dIII (stabilises CL7 and CL8 by salt bridge to R839); mutant stabilised in face-down state and all the activities were inhibited | [24] |
| D787 | D213E | 34% or 20% | 28% | 77% or 18% | | Mutation to a similar residue gives a milder but noticeable phenotype | [24,26] |
| D787 | D213G | 2% | 3% | 0% | | Important for integrity of dII and transmission of conformational changes between dII and dIII (stabilises CL7 and CL8 by salt bridge to R839); mutant stabilised in face-down state and all the activities were inhibited | [24] |
| D787 | D213H | 82% | N/A | 34% | | Mutation to a similar residue gives a milder but noticeable phenotype | [20] |
| D787 | D213I | 11% | 62% | N/A | Decreased $K_m$(NADPH) from 33 μM to 9.1 μM; decreased $S_{0.5}$ for NADPH from 2.7 to 0.27 μM in cyclic reaction | Important for integrity of dII and transmission of conformational changes between dII and dIII (stabilises CL7 and CL8 by salt bridge to R839); mutant stabilised in dIII-detached state as suggested by decreased $K_m$(NADPH) and less affected cyclic activity | [30] |
| D787 | D213K | 7% or 4% | 8% | 49% or 5% | | Important for integrity of dII and transmission of conformational changes between dII and dIII (stabilises CL7 and CL8 by salt bridge to R839); mutant stabilised in face-down state and all the activities were inhibited | [24,26] |
| D787 | D213N | 23% or 92% | 67% | 44% | Decreased $K_m$(NADPH) from 33 μM to 20 μM; decreased $S_{0.5}$ for NADPH from 2.7 to 0.43 μM in cyclic reaction | Important for integrity of dII and transmission of conformational changes between dII and dIII (stabilises CL7 and CL8 by salt bridge to R839); mutant stabilised in dIII-detached state as suggested by decreased $K_m$(NADPH) and less affected cyclic activity | [20,30] |
| D787 | D213L | 4% | 6% | 3% | | Important for integrity of dII and transmission of conformational changes between dII and dIII (stabilises CL7 and CL8 by salt bridge to R839); mutant stabilised in face-down state and all the activities were inhibited | [24] |
| D787 | D213R | 5% | 33% | 28% or 6% | | Important for integrity of dII and transmission of conformational changes between dII and dIII (stabilises CL7 and CL8 by salt bridge to R839); mutant stabilised in face-down state and all the activities were inhibited | [24,26] |
| D787 | double D213N E82Q | 25% | N/A | 81% | | | [19] |
| M788 | M214C | 50-75% | N/A | N/A | | part of CL7 and in close vicinity to dII-dIII interface | [18] |
| V790 | V216C | 50-75% | N/A | N/A | | close vicinity to proton translocation pathway | [18] |
| T793 | S219A | 100% | >120% | >120% | | close vicinity to proton translocation pathway | [24] |
| T793 | S219C | 50-75% | N/A | N/A | | close vicinity to proton translocation pathway | [18] |
| N796 | N222A | 18% or 9% | 17% or 4% | 0% or 10% | | part of proton translocation pathway; mutation to a small nonpolar residue stabilises the face-down dIII conformation, hence inhibition of all activities | [19,24,26] |
| N796 | N222C | 58% or 48% | 59% or 24% | 11% or 30% | | part of proton translocation pathway, hence proton transfer activity affected the strongest; mutation to a small uncharged residue also stabilises the face-down dIII conformation, hence intermediate inhibition of reverse and cyclic activities as well | [19,24,31] |
| N796 | N222D | 13% or 21% or 15% | 100% or 23% or 7% | 22% or 13% or 14% | | Not entirely consistent measurements, introduction of negative charge at N796 appears to favour dIII-attached conformation and favours face-down dIII | [19,24,26] |
| N796 | N222G | 2% or 11% | 2% or 5% | 0% or 10% | | part of proton translocation pathway; mutation to a small nonpolar residue stabilises the face-down dIII conformation, hence inhibition of all activities | [24,31] |
| N796 | N222H | 7% or 35% or 12% | 114% or 18% or 4% | 7% or 0% or 4% | | Different measurements not entirely consistent; N796 part of proton translocation pathway, hence proton transfer activity affected the strongest; mutation to a small uncharged residue also stabilises the face-down dIII conformation, hence intermediate inhibition of reverse and cyclic activities as well | [19,24,26] |
| N796 | N222K | 3% or 11% | 15% | 13% or 0% | retains 0.58 mol of NADP(H) per dimer | Part of proton translocation pathway next to H664; confirms observations on H91K/R mutants; low cyclic | [24,26] |

activity not entirely consistent

| | | | | | | | |
|---|---|---|---|---|---|---|---|
| N796 | N222L | 52% | 28% | 1% | | Part of proton translocation pathway next to H664; mutation to a nonpolar residue stabilises the face-down dIII conformation, hence inhibition of all activities | [24] |
| N796 | N222Q | 15% | 16% | 0% | | Part of proton translocation pathway next to H664; introduction of a larger residue stabilises the face-down dIII conformation, hence inhibition of all activities | [24] |
| N796 | N222R | 2% or 2% or 3% | 214% or 9% or 57% | 13% or 0% or 11% | retains 0.44 mol of NADP(H) per dimer | Part of proton translocation pathway next to H664; confirms observations on H91K/R mutants: dIII-detached NNT copurifies with NADP(H) and catalyses cyclic reaction | [19,24,26] |
| N796 | N222S | 3% | 1% | 0% | | Part of proton translocation pathway next to H664; mutation to a nonpolar residue stabilises the face-down dIII conformation, hence inhibition of all activities | [24] |
| N796 | N222Y | 3% or 3% | 7% or 3% | 0% or 6% | | Part of proton translocation pathway next to H664; mutation stabilises the face-down dIII conformation, hence inhibition of all activities | [19,24] |
| N796, H664 | double N222H H91N | 2% | N/A | 8% | | part of proton translocation pathway, mutant stabilised in face-down dIII conformation, underlines the sensitivity of this area to small changes | [26] |
| S797 | S223A | >120% | >120% | >120% | | not part of proton transfer pathway but in close enough vicinity to be able to distort local environment | [24] |
| Y798 | Y224F | 83% or 49% | >120% or 93% | 95% or 92% | | not part of proton transfer pathway but in close enough vicinity to be able to distort local environment | [24,31] |
| Y798 | double Y224F N222A | 8% | 5% | 10% | | not part of proton transfer pathway but in close enough vicinity to be able to distort local environment | [19] |
| S799 | S225A | 87% | 88% | 57% | | consistent with S799 participating in proton translocation as the proton translocation activity is inhibited more than hydride transfer activity in the mutant enzyme | [24] |
| S799 | S225C | ~30% | N/A | N/A | | consistent with S799 participating in proton translocation as the proton translocation activity is inhibited more than hydride transfer activity in the mutant enzyme | [18] |
| S799, S797 | double S223A S225A | 107% | N/A | 101% | | close vicinity to proton translocation pathway | [19] |
| G800 | G226A | 50% | 70% | 32% | no cyclic activity without NADPH; rev. act measured at 200 µM substrates, cyclic at 10 µM NADPH | close vicinity to proton translocation pathway | [28] |
| G807 | G233A | 49% | 31% | 30% | no cyclic activity without NADPH; rev. act measured at 200 µM substrates, cyclic at 10 µM NADPH | close vicinity to proton translocation pathway | [28] |
| N811 | S237C | 81% or >75% | >100% | N/A | | part of IL7 | [18,22] |
| N812 | N238A | 62% | N/A | 100% | | part of IL7 | [19] |
| N812 | N238C | 50% | 100% | N/A | | part of IL7 | [32] |
| N813 | D239C | 10% or 50-75% | 70% | N/A | | | [18,32] |
| L814 | L240C | 40% | 120% | N/A | | close vicinity to proton translocation pathway and part of TMH14 important for transmitting dIII-induced changes in dII | [32] |
| L815 | L241C | 40% | 60% | N/A | | close vicinity to proton translocation pathway and part of TMH14 important for transmitting dIII-induced changes in dII | [32] |
| T816 | I242C | 0% | 0% | N/A | | | [32] |
| I817 | V243C | 30% | 40% | N/A | | | [32] |
| V818 | T244C | 40% | 30% | N/A | | | [32] |
| G819 | G245C | 25% | 0% | N/A | | close vicinity to proton translocation pathway | [32] |
| G819 | G245L | 20% | 50% | N/A | | close vicinity to proton translocation pathway | [32] |
| G819 | G245A | 104% | 58% | 100% | | close vicinity to proton translocation pathway | [28] |
| A820 | A246C | 140% | 170% | N/A | | close vicinity to proton translocation pathway | [32] |

| | | | | | | | |
|---|---|---|---|---|---|---|---|
| L821 | L247C | 30% | 200% | N/A | | close vicinity to proton translocation pathway | 32 |
| I822 | V248C | 40% | 170% | N/A | | | 32 |
| G823 | G249A | 79% | 71% | 77% | | close vicinity to proton translocation pathway | 28 |
| G823 | G249C | 40% | 0% | N/A | | close vicinity to proton translocation pathway | 32 |
| G823 | G249L | 70% | 50% | N/A | | close vicinity to proton translocation pathway | 32 |
| S824 | S250A | >120% | >120% | >120% | | close vicinity to proton translocation pathway | 24 |
| S824 | S250C | 250% or >75% | 170% | N/A | Cyclic activity sensitive to phosphatase treatment | close vicinity to proton translocation pathway | 18,32 |
| S825 | S251A | >120% | >120% | 77% | | close vicinity to proton translocation pathway | 24 |
| S825 | S251C | 130% | 250% | N/A | Cyclic activity sensitive to phosphatase treatment | close vicinity to proton translocation pathway | 32 |
| S825 | double S250A S251A | 95% | N/A | 115% | | close vicinity to proton translocation pathway | 19 |
| G826 | G252A | 2.6% | 96% | 0% | Also increases NADP$^+$ independent cyclic activity by 20x – because NADPH remains bound to enzyme; measured both in membranes and purified NNT | direct contact with N796; substitution with any bulkier residue distorts the proton translocation pathway and prevents binding of dIII; consistent with co-purification with NADP(H) and high cyclic activity | 28 |
| G826 | G252C | 1.9% | 85% | 1.6% | Also increases NADP$^+$ independent cyclic activity by 20x – because NADPH remains bound to enzyme; measured both in membranes and purified NNT; Karlsson report lower (~20% cyclic activity) | direct contact with N796; substitution with any bulkier residue distorts the proton translocation pathway and prevents binding of dIII; consistent with co-purification with NADP(H) and high cyclic activity | 28,32 |
| G826 | G252S | 2.4% | 83% | 1% | Also increases NADP$^+$ independent cyclic activity by 20x – because NADPH remains bound to enzyme; measured both in membranes and purified NNT | direct contact with N796; substitution with any bulkier residue distorts the proton translocation pathway and prevents binding of dIII; consistent with co-purification with NADP(H) and high cyclic activity | 28 |
| G826 | G252T | 2.3% | 101% | 0% | Also increases NADP$^+$ independent cyclic activity by 20x – because NADPH remains bound to enzyme; measured both in membranes and purified NNT | direct contact with N796; substitution with any bulkier residue distorts the proton translocation pathway and prevents binding of dIII; consistent with co-purification with NADP(H) and high cyclic activity | 28 |
| G826 | G252V | 2.5% | 22% | 0% | Also increases NADP$^+$ independent cyclic activity by 4.5x – because NADPH remains bound to enzyme | direct contact with N796; substitution with any bulkier residue distorts the proton translocation pathway and prevents binding of dIII; consistent with co-purification with NADP(H) and high cyclic activity | 28 |
| G826 | G252L | 10% | 20% | N/A | | direct contact with N796; substitution with any bulkier residue distorts the proton translocation pathway and prevents binding of dIII; consistent with co-purification with NADP(H) and high cyclic activity | 32 |
| A827 | A253C | 50% | 150% | N/A | | close vicinity to proton translocation pathway | 32 |
| I828 | I254C | 30% | 100% | N/A | | close vicinity to proton translocation pathway | 32 |
| L829 | I255C | 80% | 150% | N/A | | | 32 |
| S830 | S256A | 89% | >120% | 95% | | close vicinity to proton translocation pathway | 24 |
| S830 | S256C | 220% | 150% | N/A | Cyclic activity sensitive to phosphatase treatment | close vicinity to proton translocation pathway | 32 |
| Y831 | Y257F | >120% | >120% | >120% | | close vicinity to proton translocation pathway | 24 |
| Y831 | Y257C | 70% | 120% | N/A | | close vicinity to proton translocation pathway | 32 |
| Y831 | double S256A Y257F | 88% | N/A | 69% | | close vicinity to proton translocation pathway | 19 |
| I832 | I258C | 70% | 80% | N/A | | important in switching dII between the two conformations; mutant switches more slowly | 32 |
| M833 | M259C | 20% | 220% | N/A | Cyclic activity not sensitive to phosphatase treatment | important in switching dII between the two conformations; mutant locked in dIII-detached conformation | 32 |
| C834 | S260C | 44% or 78% or 250% | 130% or 100% | 57% | No increase of NADP$^+$ independent cyclic activity; Karlsson et al 2003 report enchanced reverse transhydrogenation activity | Measurements not entirely consistent; this residue is important in switching dII between the two conformations | 20,23,32 |
| C834 | S260C | 23% | ~50% | N/A | done in cysteine-free NNT | important in switching dII between the two conformations | 33 |
| V835 | K261C | 8% | ~40% | N/A | done in cysteine-free NNT | | 33 |

| | | | | | | | |
|---|---|---|---|---|---|---|---|
| A836 | A262C | 8% or 50-75% | ~60% | N/A | done in cysteine-free NNT; also measured labelling of this cysteine by a maleimide MIANS; stimulated by NADP$^+$ and to a lesser degree NADPH addition | important in switching dII between the two conformations; mutant slightly stabilised in dIII-detached conformation based on cyclic activity | [18,33] |
| M837 | M263C | 5% | ~50% | N/A | done in cysteine-free NNT | important in switching dII between the two conformations; mutant slightly stabilised in dIII-detached conformation based on cyclic activity | [33] |
| N838 | N264C | 10% | ~30% | N/A | done in cysteine-free NNT | important in switching dII between the two conformations; mutant slightly stabilised in dIII-detached conformation based on cyclic activity | [33] |
| R839 | R265C | 8% | 100% | N/A | 3x higher NADP$^+$ independent cyclic activity, paradoxically increased $K_m$ for NADPH from 7 μM to 17 μM; done in cysteine-free NNT; pH optimum for reverse reaction shifted towards acidic pH (~6.5) | Maintains integrity of dII and transmits conformational changes between dII and dIII; mutant locked in dIII-detached conformation, hence reverse activity inhibited more than cyclic activity | [33] |
| R839 | R265A | 20% | ~150% | N/A | pH optimum for reverse reaction shifted towards acidic pH (~6.5) | Maintains integrity of dII and transmits conformational changes between dII and dIII; mutant locked in dIII-detached conformation, hence reverse activity inhibited more than cyclic activity | [33] |
| R839 | R265E | 8% | ~90% | N/A | pH optimum for reverse reaction shifted towards acidic pH (~6.5) | Maintains integrity of dII and transmits conformational changes between dII and dIII; mutant locked in dIII-detached conformation, hence reverse activity inhibited more than cyclic activity | [33] |
| R839 | R265K | 34% | ~130% | N/A | pH optimum for reverse reaction shifted towards acidic pH (~6.5) | Maintains integrity of dII and transmits conformational changes between dII and dIII; mutant locked in dIII-detached conformation, hence reverse activity inhibited more than cyclic activity | [33] |
| R839 | R265C AND D213C | 5% | ~30% | N/A | NADP(H)-independent cyclic activity N/A; done in cysteine-free NNT; | Maintains integrity of dII and transmits conformational changes between dII and dIII; mutant locked in dIII-detached conformation, hence reverse activity inhibited more than cyclic activity | [33] |
| S840 | S266C | 69% | ~90% | N/A | 2.4x higher NADP$^+$ independent cyclic activity, $K_m$ for NADPH 5.3 μM | not part of catalytic machinery | [33] |
| G848 | G274A | 72% | 45% | N/A | | not part of catalytic machinery | [34] |
| G848 | G274D | 50% | 63% | N/A | | not part of catalytic machinery | [34] |
| G848 | G274V | 57% | 39% | N/A | | not part of catalytic machinery | [34] |
| G850 | G276A | 60% | 42% | N/A | | not part of catalytic machinery | [34] |
| G850 | G276V | 40% | 16% | N/A | | not part of catalytic machinery | [34] |
| G850 | G276F | 41% | 29% | N/A | | not part of catalytic machinery | [34] |
| G889 | G314A | 7% or 4% | 3% or 0% | N/A | No increase of NADP$^+$ independent cyclic activity; trypsinolysis of β subunit not stimulated by NADP(H) | part of the NADP(H) binding pocket, mutation prevents NADP(H) binding, hence all activities inhibited | [23,34,35] |
| G889 | G314E | 1% | 0% | 0% | spontaneous mutation in E. coli RH1 strain; trypsinolysis of β subunit not stimulated by NADP(H) | part of the NADP(H) binding pocket, mutation prevents NADP(H) binding, hence all activities inhibited | [34–36] |
| G889 | G314C | 1% | 0% | N/A | trypsinolysis of β subunit not stimulated by NADP(H) | part of the NADP(H) binding pocket, mutation prevents NADP(H) binding, hence all activities inhibited | [34,35] |
| G889 | G314V | 1% | 0% | N/A | trypsinolysis of β subunit not stimulated by NADP(H) | part of the NADP(H) binding pocket, mutation prevents NADP(H) binding, hence all activities inhibited | [34,35] |
| Y890 | Y315H | 28% | N/A | 63% | | part of the NADP(H) binding pocket, also involved in opening of dIII | [16] |
| Y890 | Y315I | 4% | N/A | N/A | | part of the NADP(H) binding pocket, also involved in opening of dIII | [16] |
| Y890 | Y315F | 62% | N/A | 60% | Phe mutant 50% activity and pumps protons | part of the NADP(H) binding pocket, also involved in opening of dIII | [16] |
| Y890 | Y315D | 6% | N/A | N/A | | part of the NADP(H) binding pocket, also involved in opening of dIII | [16] |
| Y890 | Y315N | 25% | N/A | 20% | | part of the NADP(H) binding pocket, also involved in opening of dIII | [16] |
| Y890 | Y315V | 4% | N/A | N/A | | part of the NADP(H) binding pocket, also involved in opening of dIII | [16] |
| Y890 | Y315L | 13 | N/A | N/A | | part of the NADP(H) binding pocket, also involved in opening of dIII | [16] |
| A894 | V319G | 55% | N/A | N/A | trypsinolysis pattern the same as wild-type | | [34] |
| G912 | G337A | 68% | N/A | N/A | trypsinolysis pattern the same as wild-type | not part of catalytic machinery | [34] |
| G912 | G337D | 95% | N/A | N/A | trypsinolysis pattern the same as wild-type | not part of catalytic machinery | [34] |
| G912 | G337E | 93% | N/A | N/A | trypsinolysis pattern the same as wild-type | not part of catalytic machinery | [34] |

| | | | | | | | |
|---|---|---|---|---|---|---|---|
| G912 | double V319G G337D | 11% | N/A | N/A | trypsinolysis pattern the same as wild-type | not part of catalytic machinery | 34 |
| H920 | H345C | 250% | N/A | 26% | done in isolated dIII; retains less NADP(H) | very close to the NADP(H) binding site, destabilises nucleotide binding, making exchange possible even when not bound to dII, hence decoupled phenotype | 37 |
| H920 | H345N | 8% or 7% | 830% | 12% | additional trypsin fragment of β subunit; NADP(H)-stimulated β subunit cleavage still present | very close to the NADP(H) binding site, stimulates nucleotide binding, hence high cyclic and low reverse activities | 21,34 |
| H920 | H345Q | 18% or 17% | 22% | 30% | additional trypsin fragment of β subunit; NADP(H)-stimulated β subunit cleavage still present | very close to the NADP(H) binding site, slows down nucleotide exchange inhibiting all activities | 21,34 |
| | double G337D H345Q | 5% | N/A | N/A | fully cleaved in the absence of substrates | | 34 |
| | triple V319G G337D H345Q | 1% | N/A | N/A | | | 34 |
| A923 | A348C | 825% | N/A | 67% | done in isolated dIII; retains 60% NADPH, 34% in apo form | part of the NADP(H) binding pocket, destabilises nucleotide binding, making exchange possible even when not bound to dII, hence decoupled phenotype | 37 |
| R925 | R350C | 250% or 4% | 7% | 41% | done in isolated dIII; 24% with NADP$^+$, 30% with NADPH, 46% in apo form | part of the NADP(H) binding pocket, coordinates diphosphate; NADP(H) binding is destabilised and exchange possible even when not bound to dII, hence decoupled phenotype | 34,37 |
| R925 | R350S | 4% | 1% | N/A | | part of the NADP(H) binding pocket, coordinates diphosphate; NADP(H) binding is destabilised in mutant | 34 |
| R925 | R350G | 5% | 0% | N/A | | part of the NADP(H) binding pocket, coordinates diphosphate; NADP(H) binding is destabilised in mutant | 34 |
| R925 | double H345Q R350G | 1% | N/A | N/A | fully cleaved in the absence of substrates | Trapped in dIII-detached conformation without the nucleotide bound | 34 |
| R925 | triple V319G H345Q R350G | 1% | N/A | N/A | fully cleaved in the absence of substrates | Trapped in dIII-detached conformation without the nucleotide bound | 34 |
| R925 | triple G337D H345Q R350G | 0% | N/A | N/A | fully cleaved in the absence of substrates | Trapped in dIII-detached conformation without the nucleotide bound | 34 |
| R925 | quadruple V319G G337D H345Q R350G | 1% | N/A | N/A | fully cleaved in the absence of substrates | Trapped in dIII-detached conformation without the nucleotide bound | 34 |
| Q929 | H354Q | 10% | 78% | 10% | | | 21 |
| Q929 | H354Y | 11% | 11% | 11% | | | 21 |
| E936 | E361Q | 20% | 40% | 113% | | at the edge of the dII-dIII interface, stabilising effect on the interface, such that its formation is not strictly controlled by the nucleotide exchange, hence decoupled phenotype | 38 |
| E946 | E371Q | 71% | 78% | 34% | | at the edge of the dII-dIII interface | 38 |
| E949 | E374L | 63% | 708% | 33% | | not part of catalytic machinery; stabilises dIII in the detached state | 38 |
| D958 | D383L | 49% | 79% | N/A | | not part of catalytic machinery | 38 |
| D958 | D383R | 92% | 123% | N/A | | not part of catalytic machinery | 38 |
| A965 | A390C | 74% | 106% | N/A | | close to the NADP(H) binding site but facing away from it | 37 |
| D967 | D392C | 1375% | N/A | 18% | done in isolated dIII, fully in apo form | part of the NADP(H) binding site, also contributes to stabilisation of loop E in the closed conformation, hence nucleotide exchange possible without interaction with dII and reverse activity is elevated | 37 |
| E967 | D392A | 1% | 0% | 44% | | part of the NADP(H) binding site, prevents closing of loop E and binding of nucleotide | 38 |
| E967 | D392K | 3% | 0% | 2% | | part of the NADP(H) binding site, prevents closing of loop E and binding of nucleotide | 38 |
| E967 | D392N | 2% | 0% | 13% | | part of the NADP(H) binding site, prevents closing of loop E and binding of nucleotide | 38 |
| E967 | D392Q | 3% | 0% | 2% | | part of the NADP(H) binding site, prevents closing of loop E and binding of nucleotide | 38 |
| E967 | D392T | 2% | 0% | 2% | | part of the NADP(H) binding site, prevents closing of loop E and binding of nucleotide | 38 |
| T968 | T393C | 175% | N/A | 49% | in isolated dIII; 34% NADP$^+$, 66% NADPH; 2x faster release rate of NADPH | part of the NADP(H) binding site, hydrogen bonding with diphosphate; mutation allows nucleotide exchange to be decoupled from proton transfer, hence decoupled phenotype | 39 |

| | | | | | | | |
|---|---|---|---|---|---|---|---|
| A973 | A398C | 100% | 102% | N/A | in isolated dIII; forward reaction rate increased 3-fold | not part of catalytic machinery | [40] |
| D976 | D401G | 0-102% | 3-76% | 0-88% | | part of D loop, stabilises dI-dII linker in the face-down state | [27] |
| D976 | D401E | 0-102% | 3-76% | 0-88% | | part of D loop, stabilises dI-dII linker in the face-down state | [27] |
| D976 | D401V | 0-102% | 3-76% | 0-88% | | part of D loop, stabilises dI-dII linker in the face-down state | [27] |
| S979 | S404C | 75% | 100% | N/A | in isolated dIII; forward reaction rate increased 2-fold | part of D loop, not part of catalytic machinery | [40] |
| I981 | S406C | 450% | 29% | N/A | in isolated dIII; forward reaction rate increased 35-fold; 4x faster NADPH release | | [40] |
| G983 | G408C | 100% | 29% | N/A | in isolated dIII; forward reaction rate increased 3-fold | surface-exposed residue, not part of catalytic machinery | [40] |
| M984 | M409C | 75% | 24% | N/A | in isolated dIII; forward reaction rate increased 3-fold | close to the NADP(H) binding site | [40] |
| V986 | V411C | 125% | 31% | N/A | in isolated dIII; forward reaction rate increased 5-fold | not part of catalytic machinery | [40] |
| E988 | E413G | 70-106% | N/A | 89-99% | | surface-exposed residue, not part of catalytic machinery | [27] |
| E988 | E413D | 70-106% | N/A | 89-99% | | surface-exposed residue, not part of catalytic machinery | [27] |
| E988 | E413V | 70-106% | N/A | 89-99% | | surface-exposed residue, not part of catalytic machinery | [27] |
| K991 | K416G | 33% | 27% | 82% | | surface-exposed residue, not part of catalytic machinery | [27] |
| K999 | K424C | 425% - dI-dIII only; 30% full NNT | 50% full NNT, 45% dI/dIII | 45% | in isolated dIII; 63% apo form | part of the KRS motif of the NADP(H) binding pocket; accelerates nucleotide exchange in dI-dIII, hence faster reverse reaction but disrupts binding of NADP(H), hence slower activities measured in the full NNT | [37] |
| K999 | K424G | 1-5% | 7-36% | 0% | | KRS motif of the NADP(H) binding pocket; disrupted nucleotide binding | [27] |
| K999 | K424R | 1-5% | 7-36% | 100% | | KRS motif of the NADP(H) binding pocket; disrupted nucleotide binding | [27] |
| R1000 | R425G | 0-13% | 1-38% | 0-98% | | KRS motif of the NADP(H) binding pocket; disrupted nucleotide binding | [27] |
| R1000 | R425E | 0-13% | 1-38% | 0-98% | | KRS motif of the NADP(H) binding pocket; disrupted nucleotide binding | [27] |
| R1000 | R425K | 0-13% | 1-38% | 0-98% | | KRS motif of the NADP(H) binding pocket; disrupted nucleotide binding | [27] |
| R1000 | R425C | 425% or 10% | 8% | 12% | in isolated dIII, fully in apo form | KRS motif of the NADP(H) binding pocket; disrupted nucleotide binding | [37,39] |
| G1005 | G430C | 850% | N/A | 14% | in isolated dIII, 65% with NADPH, 32% in apo form; forward reaction rate increased ~300 fold; 110x faster NADPH release | part of the E loop important for stabilisation of the occluded state; nucleotide exchange can proceed without dII-dIII interaction, hence decoupled phenotype and accelerated reverse reaction | [39,40] |
| Y1006 | Y431C | 450% | 16% | N/A | in isolated dIII; forward reaction rate increased 100-fold; 5x faster NADPH release | part of the E loop important for stabilisation of the occluded state; nucleotide exchange can proceed without dII-dIII interaction, hence decoupled phenotype and accelerated reverse reaction | [40] |
| Y1006 | Y431H | ~3% | N/A | 11% | In full NNT | part of the E loop important for stabilisation of the occluded state | [16] |
| Y1006 | Y431L | 6% | N/A | 8% | In full NNT | part of the E loop important for stabilisation of the occluded state | [16] |
| Y1006 | Y431F | 60-80% | N/A | 19-113% | pumps protons; ~3x increase for APAD$^+$ | part of the E loop important for stabilisation of the occluded state | [16] |
| Y1006 | Y431N | 4% | N/A | N/A | | part of the E loop important for stabilisation of the occluded state | [16] |
| Y1006 | Y431I | 4% | N/A | N/A | | part of the E loop important for stabilisation of the occluded state | [16] |
| Y1006 | double Y431F Y315F | 62% | N/A | N/A | | part of the E loop important for stabilisation of the occluded state | [16] |
| Y1006 | triple alphaY226F βY315 T431 | 50% | N/A | N/A | increased $K_m$ for both substrates | part of the E loop important for stabilisation of the occluded state | [16] |
| A1007 | A432C | 150% | N/A | 63% | in isolated dIII; 78% with NADPH, 22% in apo form; forward reaction rate increased 3-fold | part of the E loop important for stabilisation of the occluded state | [39,40] |
| K1027 | K452D | 4-44% | 8-39% | 0-99% | | surface-exposed residue, not part of catalytic machinery | [27] |
| K1027 | K452G | 4-44% | 8-39% | 0-99% | | surface-exposed residue, not part of catalytic machinery | [27] |
| A1035 | K460Q | 57% | 61% | N/A | | | [41] |

| | | | | | | |
|---|---|---|---|---|---|---|
| K1036 | A461C | 46% | 57% | N/A | | [41] |
| K1036 | A461F | 42% | 70% | N/A | | [41] |
| K1036 | A461P | 48% | 59% | N/A | | [41] |
| K1036 | A461R | 86% | 118% | N/A | | [41] |
| K1036 | A461S | 69% | 93% | N/A | | [41] |
| K1036 | A461L | 68% | 86% | N/A | | [41] |
| V1037 | L462A | 38% | 55% | N/A | | [41] |
| V1037 | L462E | 47% | 70% | N/A | | [41] |
| V1037 | L462G | 58% | 86% | N/A | | [41] |
| V1037 | L462P | 37% | 52% | N/A | | [41] |
| V1037 | L462R | 37% | 45% | N/A | | [41] |
| V1037 | L462T | 62% | 102% | N/A | | [41] |
| V1037 | delta462 | 28% | 27% | N/A | | [41] |
| V1037 | delta461-462 | 3% | 2% | N/A | ~50% incorporation into membrane | [41] |
| V1037 | delta460-462 | 1% | 0% | N/A | not even incorporated into membrane | [41] |
| V1037 | delta456-462 | 1% | 1% | N/A | not even incorporated into membrane | [41] |
| V1037 | delta448-462 | 1% | 1% | N/A | not even incorporated into membrane | [41] |
| V1037 | delta442-462 | 8% | 7% | N/A | not even incorporated into membrane | [41] |
| V1037 | delta431-462 | 1% | 0% | N/A | not even incorporated into membrane | [41] |

# Supplementary Table 2. Catalytic activities of site-directed mutants in *R. rubrum* NNT

| Homologous ovine residue | *R. rubrum* mutation | Reverse activity | Cyclic activity | Proton pumping activity | Notes | Structural and mechanistic explanation if conserved | Reference |
|---|---|---|---|---|---|---|---|
| V16 | I3A | 69% | 100% | N/A | $K_d$ for NADH unchanged | | [42] |
| I108 | M97A | 62% | 98% | N/A | $K_d$ for NADH unchanged | | [42] |
| I108 | M97L | 66% | 91% | N/A | $K_d$ for NADH unchanged | | [42] |
| I108 | M97V | 72% | 112% | N/A | $K_d$ for NADH unchanged | | [42] |
| R139 | R127A | 0% | N/A | N/A | $K_m$ for NADH increases from 18 to 700-800 µM; binding of NAD$^+$ slightly weaker; E. coli R139 changes conformation between NAD$^+$ and NADH bound forms | part of the NAD(H)-binding pocket, significantly changes conformation between NAD$^+$, NADH and apo states as demonstrated in *E. coli* NNT; no NADH binding leads to complete inhibition | [43] |
| R139 | R127M | 0% | N/A | N/A | $K_m$ for NADH increases from 18 to 700-800 µM; binding of NAD$^+$ only slightly weaker; E. coli R139 changes conformation between NAD$^+$ and NADH bound forms | part of the NAD(H)-binding pocket, significantly changes conformation between NAD$^+$, NADH and apo states as demonstrated in *E. coli* NNT; no NADH binding leads to complete inhibition | [43] |
| Q144 | Q132N | 0% | 0% | N/A | hydride transfer abolished but still binds NAD(H) with approximately the same affinity | important for stabilising nicotinamide ring of NAD(H) during hydride transfer; hence complete inhibition of activities | [43,44] |
| D147 | D135N | 0% | 0% | N/A | no effect on $K_m$ of NAD(H) | immediate vicinity to the NAD(H) binding site and R139; complete inhibition suggests a role in stabilising an intermediate state | [43] |
| S150 | S138A | 0% | N/A | N/A | no effect on $K_m$ of NAD(H) | immediate vicinity to the NAD(H) binding site and R139; complete inhibition suggests a role in stabilising an intermediate state | [43] |
| Y158 | Y146A | <10% | N/A | N/A | Weaker NADH binding, purifies as a monomer | part of the dI-dI interface; strong inhibition of activity suggests that working as a dimer in anti-phase fashion is essential | [45] |
| Y158 | Y146F | 80% | N/A | N/A | | part of the dI-dI interface; only slight inhibition as dI can still dimerise | [45] |
| none | M226F | 55% | 35% | N/A | $K_d$ of NADH increases from 30 µM to 130 µM, forward reaction inhibited slightly (~30%) | | [46] |
| G241 | T231C | 58% | 90% | N/A | $K_d$ of NADH increases from 30 µM to 58 µM, forward reaction inhibited slightly (~30%) | | [46] |
| G244 | G234A | 51% | 15% | N/A | $K_d$ of NADH increases from 30 µM to 33-35 µM, forward reaction inhibited slightly (~30%) | part of the NAD(H)-binding pocket and the mobile loop; slight inhibition of activities due to weaker NAD(H) binding | [46] |
| Y245 | Y235N | ~20% | 2-3% | N/A | forward reaction inhibited by ~50%; however, reverse and forward reactions are rate-limited by product release from dIII and cyclic is rate-limited by hydride transfer | part of the NAD(H)-binding pocket and the mobile loop; almost complete inhibition of cyclic reaction, Y235 essential for stabilisation of the intermediate during hydride transfer | [47,48] |
| Y245 | Y235F | ~50% | 7-8% | N/A | forward reaction inhibited by ~50%; however, reverse and forward reactions are rate-limited by product release from dIII and cylic is rate-limited by hydride transfer | part of the NAD(H)-binding pocket and the mobile loop; almost complete inhibition of cyclic reaction, Y235 essential for stabilisation of the intermediate during hydride transfer | [47,48] |
| A246 | A236G | 72% | 53% | N/A | $K_d$ of NADH increases from 30 µM to 300-400 µM, forward reaction inhibited slightly (~30%) | part of the NAD(H)-binding pocket and the mobile loop; slight inhibition due to weaker NAD(H) binding | [46] |
| K247 | K237M | 75% | 63% | N/A | $K_d$ of NADH increases from 30 µM to 75-85 µM, forward reaction inhibited slightly (~40%) | part of the NAD(H)-binding pocket and the mobile loop; slight inhibition due to weaker NAD(H) binding | [46] |
| M258 | M239I | 80% | 30% | N/A | $K_m$ for NADH increased ~3-fold | not part of catalytic machinery | [49] |
| M258 | M239F | 58% | 16% | N/A | $K_m$ for NADH increased ~3-fold | not part of catalytic machinery | [49] |
| L353 | L343V | 69% | 95% | N/A | $K_d$ for NADH unchanged | buried residue | [42] |

## Supplementary Table 3: Missense mutations in human patients with familial glucocorticoid deficiency

| Homol-ogous ovine residue | *Human* mutation | Reverse activity | Cyclic activity | Proton pumping activity | Notes | Structural and mechanistic explanation if conserved | Reference |
|---|---|---|---|---|---|---|---|
| S150 | S150N | N/A | N/A | N/A | | immediate vicinity of the NAD(H) binding pocket | [50] |
| G157 | G157S | N/A | N/A | N/A | more severe phenotype, includes mineralocorticoid deficiency | immediate vicinity of the NAD(H) binding pocket | [51] |
| F172 | F172S | N/A | N/A | N/A | | part of the dI-dI interface | [52] |
| M294 | M294V | N/A | N/A | N/A | | buried residue | [53] |
| T314 | T314A | N/A | N/A | N/A | | buried residue | [50] |
| Y345 | Y345S | N/A | N/A | N/A | | buried residue, relatively close to the dI-dI interface | [54] |
| P394 | P394L | N/A | N/A | N/A | | surface exposed residue, immediate vicinity to the dI-dII linker | [50,53] |
| A490 | A490V | N/A | N/A | N/A | | immediate vicinity to the proton translocation pathway | [50] |
| G621 | G621R | N/A | N/A | N/A | | buried residue | [50] |
| G635 | G635R | N/A | N/A | N/A | | membrane-facing residue | [50] |
| G819 | G819D | N/A | N/A | N/A | | close vicinity to the proton translocation pathway | [50] |
| A820 | A820E | N/A | N/A | N/A | More severe phenotype with hypoglycaemia and precocious puberty | close vicinity to the proton translocation pathway | [53] |
| L934 | L934P | N/A | N/A | N/A | | part of the conserved helix 4 important for dII-dIII interface formation | [50] |
| A965 | A965P | N/A | N/A | N/A | | forms the NADP(H)-binding pocket | [50] |
| N966 | N966K | N/A | N/A | N/A | | forms the NADP(H)-binding pocket | |

# References

1.  Leung, J. H. *et al.* Structural biology. Division of labor in transhydrogenase by alternating proton translocation and hydride transfer. *Science* **347**, 178–81 (2015).

2.  Padayatti, P. S. *et al.* Critical Role of Water Molecules in Proton Translocation by the Membrane-Bound Transhydrogenase. *Structure* 1–9 (2017).

3.  Yamaguchi, M., Wakabayashi, S. & Hatefi, Y. Mitochondrial Energy-Linked Nicotinamide Nucleotide Transhydrogenase: Effect of Substrates on the Sensitivity of the Enzyme to Trypsin and Identification of Tryptic Cleavage Sites. *Biochemistry* **29**, 4136–4143 (1990).

4.  Venning, J. D., Peake, S. J., Quirk, P. G. & Jackson, J. B. Stopped-flow reaction kinetics of recombinant components of proton-translocating transhydrogenase with physiological nucleotides. *J. Biol. Chem.* **275**, 19490–7 (2000).

5.  Venning, J. D., Bizouarn, T., Cotton, N. P. J., Quirk, P. G. & Jackson, J. B. Stopped-flow kinetics of hydride transfer between nucleotides by recombinant domains of proton-translocating transhydrogenase. *Eur. J. Biochem.* **257**, 202–209 (1998).

6.  Hutton, M., Day, J. M., Bizouarn, T. & Jackson, J. B. Kinetic resolution of the reaction catalysed by proton-translocating transhydrogenase from Escherichia coli as revealed by experiments with analogues of the nucleotide substrates. *Eur. J. Biochem.* **219**, 1041–1051 (1994).

7.  Cotton, N. P. J., White, S. A., Peake, S. J., Mcsweeney, S. & Jackson, J. B. The Crystal Structure of an Asymmetric Complex of the Two Nucleotide Binding Components of Proton-Translocating Transhydrogenase. *Structure* **9**, 165–176 (2001).

8.  Sundaresan, V., Chartron, J., Yamaguchi, M. & Stout, C. D. Conformational Diversity in NAD(H) and Interacting Transhydrogenase Nicotinamide Nucleotide Binding Domains. *J. Mol. Biol.* **346**, 617–629 (2005).

9.  Singh, A. *et al.* Interactions between transhydrogenase and thio-nicotinamide analogues of NAD(H) and NADP(H) underline the importance of nucleotide conformational changes in coupling to proton translocation. *J. Biol. Chem.* **278**, 33208–33216 (2003).

10. Mather, O. C., Singh, A., Van Boxel, G. I., White, S. A. & Jackson, J. B. Active-site conformational changes associated with hydride transfer in proton-translocating transhydrogenase. *Biochemistry* **43**, 10952–10964 (2004).

11. Cooley, R. B., Arp, D. J. & Karplus, P. A. Evolutionary Origin of a Secondary Structure: π-Helices as Cryptic but Widespread Insertional Variations of α-Helices That Enhance Protein Functionality. *J. Mol. Biol.* **404**, 232–246 (2010).

12. Efremov, R. G. & Sazanov, L. A. Structure of the membrane domain of respiratory complex i. *Nature* **476**, 414–421 (2011).

13. Prasad, G. S. *et al.* Crystal structures of transhydrogenase domain I with and without bound NADH. *Biochemistry* **41**, 12745–12754 (2002).

14. Johansson, T. *et al.* X-ray structure of domain I of the proton-pumping membrane protein transhydrogenase from Escherichia coli. *J. Mol. Biol.* **352**, 299–312 (2005).

15. Hu, X., Zhang, J. & Rydström, J. Interactions of reduced and oxidized nicotinamide mononucleotide with wild-type and αD195E mutant proton-pumping nicotinamide nucleotide transhydrogenases from Escherichia coli. *Biochim. Biophys. Acta -*

*Bioenerg.* **1367**, 134–138 (1998).

16.	Olausson, T. *et al.* Site-directed mutagenesis of tyrosine residues at nicotinamide nucleotide binding sites of Escherichia coli transhydrogenase. *Biochemistry* **32**, 13237–13244 (1993).

17.	Glavas, N., Ahmad, S., Bragg, P. D., Olausson, T. & Rydström, J. Identification of N,N'-dicyclohexylcarbodiimide-reactive glutamic and aspartic acid residues in Escherichia coli transhydrogenase and the exchange of these by site-specific mutagenesis. *J. Biol. Chem.* **268**, 14125–30 (1993).

18.	Meuller, J. & Rydström, J. The membrane topology of proton-pumping Escherichia coli transhydrogenase determined by cysteine labeling. *J. Biol. Chem.* **274**, 19072–19080 (1999).

19.	Bragg, P. D. & Hou, C. Mutation of conserved polar residues in the transmembrane domain of the proton-pumping pyridine nucleotide transhydrogenase of Escherichia coli. *Arch Biochem Biophys* **363**, 182–190 (1999).

20.	Holmberg, E. *et al.* Prediction and site-specific mutagenesis of residues in transmembrane alpha-helices of proton-pumping nicotinamide nucleotide transhydrogenases from Escherichia coli and bovine heart mitochondria. *Biochemistry* **33**, 7691–700 (1994).

21.	Bragg, P. D. & Hou, C. The Role of Conserved Histidine Residues in the Pyridine Nucleotide Transhydrogenase of Escherichia Coli. *Eur. J. Biochem.* **241**, 611–618 (1996).

22.	Althage, M. *et al.* Cross-linking of transmembrane helices in proton-translocating nicotinamide nucleotide transhydrogenase from Escherichia coli: implications for the structure and function of the membrane domain. *Biochim. Biophys. Acta - Bioenerg.* **1659**, 73–82 (2004).

23.	Glavas, N. A. & Bragg, P. D. The mechanism of hydride transfer between NADH and 3-acetylpyridine adenine dinucleotide by the pyridine nucleotide transhydrogenase of Escherichia coli. *Biochim. Biophys. Acta* **1231**, 297–303 (1995).

24.	Yamaguchi, M., Stout, D. C. & Hatefi, Y. The proton channel of the energy-transducing nicotinamide nucleotide transhydrogenase of Escherichia coli. *J. Biol. Chem.* **277**, 33670–33675 (2002).

25.	Glavas, N. A., Hou, C. & Bragg, P. D. Involvement of Histidine-91 of the β Subunit in Proton Translocation by the Pyridine Nucleotide Transhydrogenase of Escherichia coli. *Biochemistry* **34**, 7694–7702 (1995).

26.	Bragg, P. D. & Hou, C. Characterization of mutants of βHistidine91, βAspartate213, and βAsparagine222, possible components of the energy transduction pathway of the proton-translocating pyridine nucleotide transhydrogenase of Escherichia coli. *Arch. Biochem. Biophys.* **388**, 299–307 (2001).

27.	Hu, X., Zhang, J., Fjellström, O., Bizouarn, T. & Rydström, J. Site-directed mutagenesis of charged and potentially proton-carrying residues in the β subunit of the proton-translocating nicotinamide nucleotide transhydrogenase from escherichia coli. Characterization of the βH91, βD392, and βK424 mutants. *Biochemistry* **38**, 1652–1658 (1999).

28.	Yamaguchi, M. & Stout, C. D. Essential Glycine in the Proton Channel of Escherichia coli Transhydrogenase. *J. Biol. Chem.* **278**, 45333–45339 (2003).

29. Althage, M. *et al.* Functional split and crosslinking of the membrane domain of the β subunit of proton-translocating transhydrogenase from Escherichia coli. *Biochemistry* **42**, 10998–11003 (2003).

30. Yamaguchi, M. & Hatefi, Y. Proton-translocating nicotinamide nucleotide transhydrogenase of Escherichia coli. Involvement of aspartate 213 in the membrane-intercalating domain of the beta subunit in energy transduction. *J. Biol. Chem.* **270**, 16653–16659 (1995).

31. Bragg, P. D. & Hou, C. Mutation of conserved polar residues in the transmembrane domain of the proton-pumping pyridine nucleotide transhydrogenase of Escherichia coli. *Arch Biochem Biophys* **363**, 182–190 (1999).

32. Karlsson, J., Althage, M. & Rydström, J. Roles of individual amino acids in helix 14 of the membrane domain of proton-translocating transhydrogenase from Escherichia coli as deduced from cysteine mutagenesis. *Biochemistry* **42**, 6575–6581 (2003).

33. Althage, M., Bizouarn, T. & Rydström, J. Identification of a region involved in the communication between the NADP(H) binding domain and the membrane domain in proton pumping E. coli transhydrogenase. *Biochemistry* **40**, 9968–9976 (2001).

34. Bragg, P. D., Glavas, N. A. & Hou, C. Mutation of Conserved Residues in the NADP(H)-Binding Domain of the Proton Translocating Pyridine Nucleotide Transhydrogenase ofEscherichia coli. *Arch. Biochem. Biophys.* **338**, 57–66 (1997).

35. Ahmad, S., Glavas, N. A. & Bragg, P. D. A mutation at Gly314 of the β subunit of the Escherichia coli pyridine nucleotide transhydrogenase abolishes activity and affects the NADP(H)-induced conformational change. *Eur. J. Biochem.* **207**, 733–739 (1992).

36. Johansson, C., Bergkvist, A., Fjellström, O., Rydström, J. & Karlsson, B. G. Sequential assignment and secondary structure analysis of the NADP(H)-binding domain of Escherichia coli transhydrogenase. *J. Biomol. NMR* **14**, 295–6 (1999).

37. Fjellström, O. *et al.* Mapping of residues in the NADP(H)-binding site of proton-translocating nicotinamide nucleotide transhydrogenase from Escherichia coli. A study of structure and function. *J. Biol. Chem.* **274**, 6350–6359 (1999).

38. Meuller, J., Hu, X., Bunthof, C., Olausson, T. & Rydström, J. Identification of an aspartic acid residue in the β subunit which is essential for catalysis and proton pumping by transhydrogenase from Escherichia coli. *Biochim. Biophys. Acta - Bioenerg.* **1273**, 191–194 (1996).

39. Bergkvist, A., Johansson, C., Johansson, T., Rydstrom, J. & Karlsson, B. G. Interactions of the NADP(H)-binding domain III of proton-translocating transhydrogenase from Escherichia coli with NADP(H) and the NAD(H)-binding domain I studied by NMR and site-directed mutagenesis. *Biochemistry* **39**, 12595–12605 (2000).

40. Johansson, C., Pedersen, A., Karlsson, B. G. & Rydström, J. Redox-sensitive loops D and E regulate NADP(H) binding in domain III and domain I-domain III interactions in proton-translocating Escherichia coli transhydrogenase. *Eur. J. Biochem.* **269**, 4505–4515 (2002).

41. Bragg, P. D. & Hou, C. Effect of truncation and mutation of the carboxyl-terminal region of the β subunit on membrane assembly and activity of the pyridine nucleotide transhydrogenase of Escherichia coli. *Biochim. Biophys. Acta - Bioenerg.* **1365**, 464–472 (1998).

42. Tveen Jensen, K., Strambini, G., Gonnelli, M., Broos, J. & Jackson, J. B. Mutations in Transhydrogenase Change the Fluorescence Emission State of TRP72 from 1La to 1Lb. *Biophys. J.* **95**, 3419–3428 (2008).

43. Brondijk, T. H. C. *et al.* The role of invariant amino acid residues at the hydride transfer site of proton-translocating transhydrogenase. *J. Biol. Chem.* **281**, 13345–13354 (2006).

44. Van Boxel, G. I., Quirk, P. G., Cotton, N. P. J., White, S. A. & Jackson, J. B. Glutamine 132 in the NAD(H)-binding component of proton-translocating transhydrogenase tethers the nucleotides before hydride transfer. *Biochemistry* **42**, 1217–1226 (2003).

45. Obiozo, U. M. *et al.* Substitution of tyrosine 146 in the dI component of proton-translocating transhydrogenase leads to reversible dissociation of the active dimer into inactive monomers. *J. Biol. Chem.* **282**, 36434–36443 (2007).

46. Gupta, S. *et al.* Mutation of amino acid residues in the mobile loop region of the NAD(H)-binding domain of proton-translocating transhydrogenase. *Biochim. Biophys. Acta - Bioenerg.* **1409**, 25–38 (1998).

47. Diggle, C. *et al.* Mutation of Tyr235 in the NAD(H)-binding subunit of the proton-translocating nicotinamide nucleotide transhydrogenase of Rhodospirillum rubrum affects the conformational dynamics of a mobile loop and lowers the catalytic activity of the enzyme. *J. Biol. Chem.* **271**, 10109–15 (1996).

48. Bizouarn, T., Grimley, R., Diggle, C., Thomas, C. M. & Jackson, J. B. Mutations at tyrosine-235 in the mobile loop region of domain I protein of transhydrogenase from Rhodospirillum rubrum strongly inhibit hydride transfer. *Biochim. Biophys. Acta - Bioenerg.* **1320**, 265–274 (1997).

49. Grimley, R. L., Quirk, P. G., Bizouarn, T., Thomas, C. M. & Jackson, J. B. Role of methionine-239, an amino acid residue in the mobile-loop region of the NADH-binding domain (domain I) of proton-translocating transhydrogenase. *Biochemistry* **36**, 14762–14770 (1997).

50. Meimaridou, E. *et al.* Mutations in NNT encoding nicotinamide nucleotide transhydrogenase cause familial glucocorticoid deficiency. *Nat. Genet.* **44**, 740–2 (2012).

51. Weinberg-Shukron, A. *et al.* Combined mineralocorticoid and glucocorticoid deficiency is caused by a novel founder nicotinamide nucleotide transhydrogenase mutation that alters mitochondrial morphology and increases oxidative stress. *J. Med. Genet.* **52**, 636–641 (2015).

52. Yamaguchi, R. *et al.* A novel homozygous mutation of the nicotinamide nucleotide transhydrogenase gene in a Japanese patient with familial glucocorticoid deficiency. *Endocr. J.* **60**, 855–859 (2013).

53. Roucher-Boulez, F. *et al.* NNT mutations: a cause of primary adrenal insufficiency, oxidative stress and extra- adrenal defects. *Eur. J. Endocrinol.* **175**, 73–84 (2016).

54. Hershkovitz, E., Arafat, M., Loewenthal, N., Haim, A. & Parvari, R. Combined adrenal failure and testicular adrenal rest tumor in a patient with nicotinamide nucleotide transhydrogenase deficiency. *J. Pediatr. Endocrinol. Metab.* **28**, 1187–90 (2015).